CHAPTER 9

FLOW AND TRANSPORT IN THE UNSATURATED ZONE

MANAR EL-BESHRY

9.1 CAPILLARY ACTION

Flow and transport mechanisms in the unsaturated zone are much more complex than in the saturated zone due to the effect of capillary forces and nonlinear soil characteristics. In an unsaturated porous medium, part of the pore space is filled with water and part is filled with air, and the total porosity is defined as the sum of the two moisture contents:

$$n = \theta_w + \theta_a \tag{9.1}$$

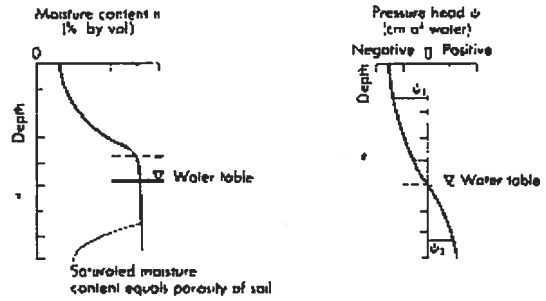

Figure 9.1 Typical θ and ψ relationships with depth in the unsaturated zone.

The moisture content θ_w is defined as the ratio of the volume of water to the total volume of porous media sample, and θ_a is the ratio of the volume of air to the total volume of porous media. The unsaturated or vadose zone constitutes that part of the soil profile where water content is less than the soil porosity, and where the soil water pressure is negative. The water-saturated capillary fringe just above the water table is also considered part of the unsaturated zone.

Figure 9.1 shows the variation of moisture content and pressure head ψ with depth. Near the water table a capillary fringe can occur where ψ is a small negative pressure corresponding to the air entry pressure. In this zone, the pores are saturated but the pressure is slightly less than atmospheric. This capillary zone is small for sandy soils but can be up to two meters for fine grained soils. By definition, pressure head is negative (under tension) at all points above the water table and is positive for points below the water table. The value of ψ is greater than zero in the saturated zone below the water table and equals zero at the water table. Soil physicists refer to $\psi < 0$ as the tension head or capillary suction head, which can be measured by an instrument called a tensiometer (Section 9.5).

The water that is in the unsaturated zone is adsorbed as a film on the surface of the grains, held strongly by suction pressure. As more water is added to the porous structure, water movement is restricted due to the strong sorption and capillary forces. Eventually, a continuous wetting phase will form, and the air can become trapped in the larger pores, thus restricting the air phase. Full water saturation is generally not achieved in the unsaturated zone because of the trapped residual air.

One can consider actual porous media to be similar to a bundle of thin glass tubes of radius r. A curved surface will tend to develop at the interface between water and air and the difference in pressure across the interface is called **capillary pressure**, and is directly proportional to the interfacial tension and inversely proportional to the radius of curvature. The capillary pressure P in a thin tube can be determined from a balance between the weight of the water column in the tube and capillary forces pulling upward, or

$$P = \frac{2\sigma \cos\gamma}{r} \tag{9.2}$$

where σ is the interfacial tension, r is the radius of the tube, and γ is the interface angle between the two liquids. Capillary forces and wettability of a fluid, the tendency of the fluid to preferentially spread over a solid surface, is described in detail in Section 11.3.

9.2 SOIL-WATER CHARACTERISTIC CURVES

Hydraulic conductivity $K(\theta)$ relates velocity and hydraulic gradient in Darcy's law. Moisture content θ is defined as the ratio of the volume of water to the total volume of a unit of porous media. To complicate the analysis of unsaturated flow, both θ and K are functions of the capillary suction ψ. Also, it has been observed experimentally that the θ–ψ relationships differ significantly for different types of soil. Figure 9.2a shows the characteristic drying and wetting curves that occur in soils that are draining water or receiving infiltration of water. The nonlinear nature of these curves for several selected soils are shown in Figure 9.2b. The curves reflect the fact that the hydraulic conductivity and moisture content of an unsaturated soil increase with decreasing capillary suction. The sandier soils show a very different response compared to the tighter loam and clay soils.

At atmospheric pressure, the soil is saturated with water content equal to θ_s. The soil will initially remain saturated as the capillary pressure (matric potential) is gradually decreased. Eventually, water will begin to drain from the soil as the pressure is lowered, and the moisture content will continue to decline until it reaches some minimum water content θ_r. Further reductions in the capillary pressure will not result in any additional moisture, as shown in Figure 9.2a. Thus the sandier soils are drained (or lose moisture) more quickly than the tighter soils. This is due to the fact that the sands have larger pores.

Some simple empirical expressions used to relate water content of a soil to the capillary pressure head include the one from Brooks and Corey (1964)

$$\theta = \theta_r + (\theta_s - \theta_r)(\psi/\psi_b)^{-\lambda} \tag{9.3}$$

where

θ = volumetric water content
θ = volumetric water content at saturation
θ_r = irreducible minimum water content
ψ = matric potential or capillary suction
ψ_b = bubbling pressure
λ = experimentally derived parameter

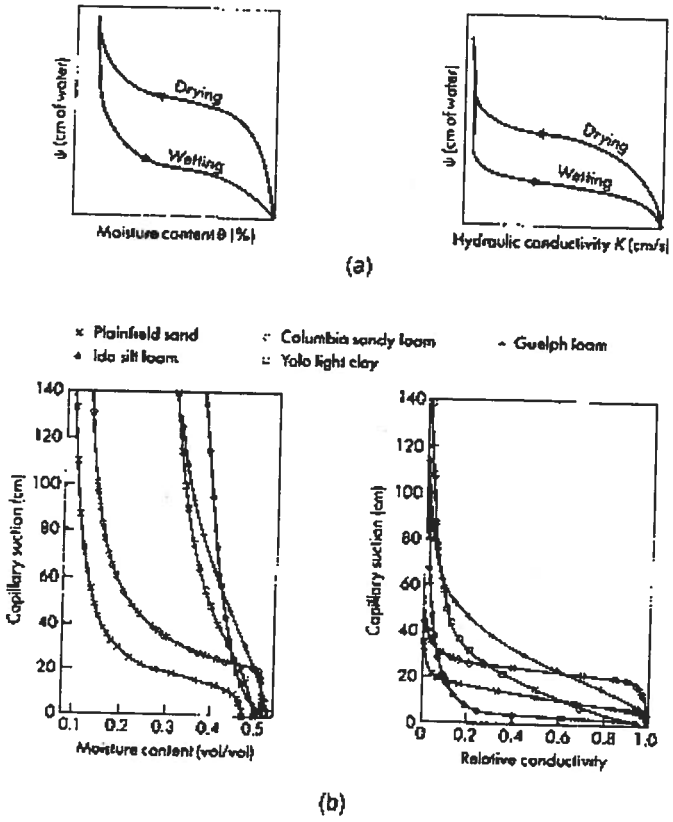

Figure 9.2 Soil characteristic curves for (a) wetting and drying and (b) different soil types

Brooks and Corey (1964) also defined an effective saturation, S_e, as

$$S_e = \frac{S_w - \theta_r}{1 - \theta_r} \tag{9.4}$$

where $S_w = \theta/\theta_s$, the saturation ratio.

Van Genuchten (1980) also derived an empirical relationship between capillary pressure head and volumetric water content, defined by

$$\theta = \theta_r + \frac{\theta_s - \theta_r}{\left[1 + (\alpha\psi)^n\right]^m} \tag{9.5}$$

where α, m, and n are constants. Generally, these equations work well for medium- and coarse-textured soils with predictions for fine-textured materials usually being less accurate. These equations are often used in computer models to represent soil characteristics for flow in the unsaturated zone. For large capillary heads, the Brooks and Corey and Van Genuchten models become identical if $\lambda = mn$ and $\psi_b = 1/\alpha$.

A drying curve occurs when one allows an initially saturated sample to desorb water by applying suction. If the sample is then resaturated with water, thus decreasing the suction, it will follow a wetting curve. The fact that the drying curve and the wetting curve will generally not be the same produces the hysteretic behavior of the soil water retention curve as illustrated in Figure 9.3. The soil water content is not a unique function of capillary pressure, but depends on the previous history of the soil. The hysteretic nature of θ is due to the presence of different contact angles during wetting and drying cycles, and to geometric restrictions of single pores (Nielsen et al., 1986). For example, the contact angle between the water and the soil surface is greater during the advance of a water front than during its retreat.

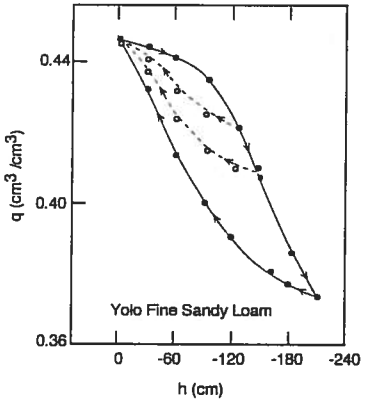

Figure 9.3 Water retention curves for a sample of Yolo fine, sandy loam. The solid curves are eye-fitted through measured data along the two main boundary curves. Dashed curves represent primary wetting scanning curves. Arrows indicate the direction at which the pressure head changes are imposed. Source: Nielson et al., 1986. © American Geophysical Union.

Air trapped in pores during a wetting cycle will reduce the water content of a soil during wetting, but eventually that trapped air will dissolve. Hysteresis effects are usually augmented by the presence of trapped air, and soil shrinking and swelling (Davidson et al., 1966). Hysteresis creates a significant problem for the prediction of flow rates and transport phenomena in the unsaturated zone.

.3 UNSATURATED HYDRAULIC CONDUCTIVITY

Evidence suggests that Darcy's law is still valid for unsaturated flow except that hydraulic conductivity is now a function of moisture content. Darcy's law is then used with the unsaturated value for K and can be written

$$v = -K(\theta)\partial h/\partial z \tag{9.6}$$

where v is darcy velocity, z is depth below surface [L], ψ is tension or suction [L], $K(\theta)$ is unsaturated hydraulic conductivity [L/T], h is potential or head ($h = z + \psi$) [L/T], and θ is volumetric moisture content.

Unsaturated hydraulic conductivity can be determined by both field methods and laboratory techniques, both of which are time-consuming and tedious. Estimates are often made from soil parameters obtained from soil-water retention relationships such as those from Brooks and Corey (1964) and Van Genuchten (1980). Figure 9.4 shows observed values and calculated curves for relative hydraulic conductivity as a function of capillary pressure.

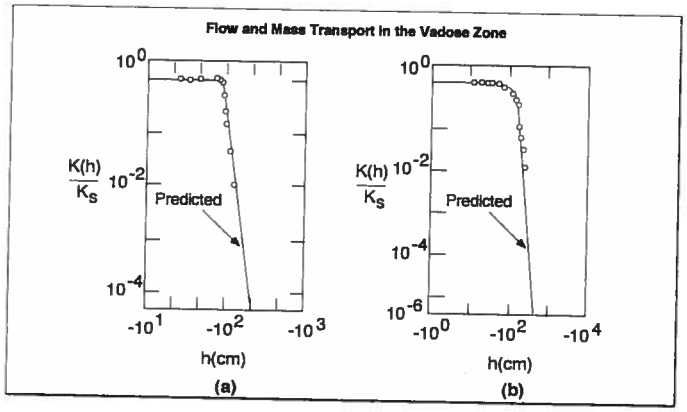

Figure 9.4 Observed values (open circles) and calculated curves (solid lines) for relative hydraulic conductivity of (a) Hygiene sandstone and (b) Touchet silt loam. Source: Van Genuchten, 1980.

9.4 GOVERNING EQUATION FOR UNSATURATED FLOW

The water table defines the boundary between the unsaturated and saturated zones and is defined by the surface at which the fluid pressure P is exactly atmospheric, or $P = 0$. Hence, the total hydraulic head $h = \psi + z$, where $\psi = P/\rho g$, the capillary pressure head.

Considerations of unsaturated flow include the solution of the governing equation of continuity and Darcy's law in an unsaturated porous media. The governing equation, originally derived by Richard in 1931, is based on substituting Darcy's law Eq. (9.6) into the unsaturated continuity equation,

$$-\left[\frac{\partial(\rho v_x)}{\partial x} + \frac{\partial(\rho v_y)}{\partial y} + \frac{\partial(\rho v_z)}{\partial z}\right] = \frac{\partial}{\partial t}\rho\theta \tag{9.7}$$

The resulting equation is

$$\frac{\partial\theta}{\partial t} = -\frac{\partial}{\partial z}\left[K(\theta)\frac{\partial\psi(\theta)}{\partial z}\right] - \frac{\partial K(\theta)}{\partial z} \tag{9.8}$$

where

θ = volumetric moisture content
z = distance below the surface [L]
θ = capillary suction (pressure) [L of water]
$K(\theta)$ = unsaturated hydraulic conductivity [L/T]

Equation (9.8) is called Richards (1931) equation and is a nonlinear partial differential equation that is quite difficult to solve. The Richards equation assumes that the presence of air can be ignored, that water is incompressible, and that the soil matrix is nondeformable. Both numerical and analytical solutions exist for certain special cases. The most difficult part of the procedure is determining the characteristic curves for a soil (Figure 9.2). The characteristic curves reduce to the fundamental hydraulic parameters K and n in the saturated zone and remain as functional relationships in the unsaturated zone.

A number of analytical and numerical solution techniques have been developed over the last 35 years for Eq. (9.8). Analytical approaches require greatly simplified conditions for boundaries, and are generally restricted to 1-D vertical systems. Early work by Philip and de Vries (1957) provided much of the physical and mathematical ground work for subsequent analyses. The analytical approaches are useful for deriving physically based expressions for infiltration rates in unsaturated soils. A more recent approach based on the method of characteristics has been applied to gravity-dominated flow in the unsaturated zone (Smith 1983; Charbeneau, 1984).

Charbeneau (1984) considers the kinematic theory of soil moisture and solute transport in the vertical direction for unsaturated ground water recharge. It is assumed that the soil starts at and eventually drains to field capacity. Analytical expressions are developed for water content and moisture flux as a function of depth and time, and the approach is extended for an arbitrary sequence of surface boundary conditions. In this approach, dissipative terms are neglected in the governing equations, thus allowing the powerful method of characteristics to be used in the solution. Numerical methods are more suited to handling actual laboratory and field situations. Finite difference methods were proposed by Rubin and Steinhardt (1963) and Freeze (1969, 1971). Finite difference numerical techniques are presented in detail in this chapter for flow and transport in the unsaturated zone.

There are two extreme cases which should be considered. For large values of moisture content, $\partial\psi/\partial\theta$ is approximately zero and the continuity equation becomes

$$\frac{\partial\theta}{\partial t} = -\frac{\partial K(\theta)}{\partial z} \tag{9.9}$$

Equation (9.9) leads to the kinematic theory of modeling the unsaturated flow, where capillary pressure gradients are neglected. The theory is also applicable if ψ=CONSTANT within the profile. Thus, Darcy's law predicts that flow is downward under a unit gradient. The second extreme case occurs when capillary forces completely dominate gravitational forces, resulting in a nonlinear diffusion equation. This latter form is useful for modeling evaporation processes.

To summarize the properties of the unsaturated zone as compared to the saturated zone, Freeze and Cherry (1979) state that:

For the unsaturated zone (vadose zone):

1. It occurs above the water table and above the capillary fringe.
1. The soil pores are only partially filled with water; the moisture content θ is less than the porosity n.
3. The fluid pressure P is less than atmospheric; the pressure head ψ is less than zero.
4. The hydraulic head h must be measured with a tensiometer.
5. The hydraulic conductivity K and the moisture content θ are both functions of the pressure head ψ.

For the saturated zone:

1. It occurs below the water table.
2. The soil pores are filled with water; and the moisture content θ equals the porosity n.

3. The fluid pressure P is greater than atmospheric, so the pressure head ψ (measured as gauge pressure) is greater than zero.
4. The hydraulic head h must be measured with a piezometer.
5. The hydraulic conductivity K is not a function of the pressure head ψ.

Finally, more details on the unsaturated zone can be found in Fetter (1999), Rawls et al. (1993), Charbeneau and Daniel (1993) and Guyman (1994).

9.5 MEASUREMENT OF SOIL PROPERTIES

Moisture characteristic curves for a particular soil can be determined by any of three approaches (Charbeneau and Daniel, 1993). The first technique is to estimate the curve (water content versus capillary pressure head) from published data for similar soils. For example, Rawls et al. (1983) collected and analyzed data from over 500 soils. Gupta and Larson (1979) describe the use of grain-size distribution data, organic content, and bulk density to estimate moisture characteristic curves. The second technique is to assume an analytic function such as that of Brooks and Corey (1964) or Van Genuchten (1980). These equations were presented in Section 9.2. The empirical coefficients in these functions are usually estimated based on correlations of various soil characteristics.

The third approach is to actually measure the soil moisture characteristic curve directly. Incremental equilibrium methods allow the soil to come to equilibrium at some moisture content θ, and then capillary pressure ψ is measured. Next θ is changed and time is allowed for equilibrium to reestablish and ψ is remeasured. The process is repeated until a sufficient number of ψ–θ points have been measured to define the entire curve (Figure 9.2). One can also allow ψ to come to equilibrium and measure θ for changes in ψ. The pressure plate is the most commonly used method of measurement and involves placing a chamber around soil samples that have been soaked with water. Positive air pressure is used to force water out of the soil samples and the outflow is monitored to confirm equilibrium. After equilibrium is established, the chamber is disassembled, and the soil samples are oven dried to determine θ.

Hydraulic conductivity in unsaturated soils is determined from K_s, the value at saturation and the relative permeability k_r, which is a function of capillary pressure head, volumetric water content or degree of water saturation. The relative permeability k_r can be estimated from other soil properties or can be directly measured in the laboratory. Klute and Dirksen (1986) summarize several methods of unsaturated hydraulic conductivity in the laboratory. They report on steady state methods for a steady flow through a soil column with controlled pressure at both ends of the column. This technique is not practical for soils with low K because the flow rate cannot be measured accurately. Olson and Daniel (1986) report on transient tests where soil is placed in a pressure plate device, a step increase in air pressure is

imposed, the rate of water flow out of the soil is measured versus time, and K is computed from the resulting data.

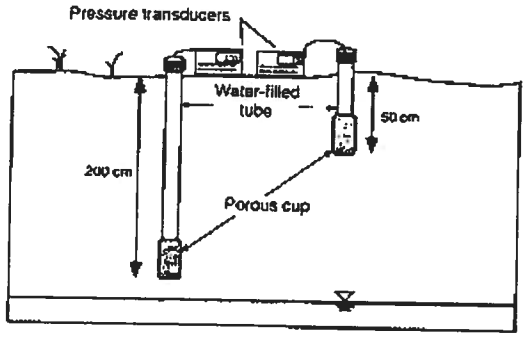

Figure 9.5 Two tensiometers used to determine the gradient of the soil-water potential.

Hydraulic conductivity at saturation K_s is measured in the laboratory using rigid-wall permeameters and flexible-wall permeameters. Hydraulic conductivity tests may be performed with a constant head, falling head or constant flux (Olson and Daniel, 1986; Klute and Dirksen, 1986). Differences have been noted between laboratory determined values and those estimated from field tests. Olson and Daniel compared laboratory and field measured K_s values for 72 data sets involving clayey soils and found significant differences, since hydraulic conductivity tends to increase with increasing scale of measurement relating to structural features of the soil.

Capillary pressure head can be measured in an undisturbed soil sample in the laboratory or the measurement can be obtained in the field. In both cases, a tensiometer, consisting of a porous element inserted into the soil and a pressure sensing device at the surface, is often used. The tensiometer is initially saturated with a liquid and when brought into contact with the soil, and the soil will pull water out of the tensiometer creating a negative pressure, that can be measured (Charbeneau and Daniel, 1993). A tensiometer generally cannot read more negative than 0.9 bar due to problems of cavitation of water. Figure 9.5 depicts a tensiometer for field use.

6 INFILTRATION MODELS

Infiltration is the process of vertical movement of water into a soil from rainfall, snowmelt, or irrigation. Infiltration of water plays a key role in surface runoff, ground water recharge, evapotranspiration, and transport of chemicals into the subsurface. Models to characterize

infiltration for field applications usually employ simplified concepts that predict the infiltration rate assuming surface ponding begins when the surface application rate exceeds the soil infiltration rate. Empirical, physically based, and physical models have all been developed for the infiltration process. A more detailed review of infiltration can be found in Rawls et al. (1993).

Richards Equation, Eq. (9.8), is the physically based infiltration equation used for describing water flows in soils. Philip (1957) solved the equation analytically for the condition of excess water at the surface and given characteristic curves. Their coefficients can be predicted in advance from soil properties and do not have to be fitted to field data. However, the more difficult case where the rainfall rate is less than the infiltration capacity cannot be handled by Philip's equation. Another limitation is that it does not hold valid for extended time periods. Swartzendruber (1987) presented a solution to Richards equation that holds for both small, intermediate and large times.

A number of operational infiltration models have been developed over the years and are covered in detail in hydrology textbooks such as Chow, et al. (1988), Bedient and Huber (1992), and Rawls et al. (1993). These include the SCS runoff curve number method, the Horton method, and the Holtan method (SCS, 1986; Horton, 1940; Holtan, 1961).

One of the most interesting and useful approaches to solving the governing equation for infiltration was originally advanced by Green and Ampt (1911). In this method, water is assumed to move into dry soil as a sharp wetting front that separates the wetted and unwetted zones. At the location of the front, the average capillary suction head $\psi = \psi_f$, is used to represent the characteristic curve. The moisture content profile at the moment of surface saturation is shown in Figure 9.6a. The area above the moisture profile is the amount of infiltration up to surface saturation F and is represented by the shaded area of depth L in Figure 9.6a. Thus, $F = (\theta_s - \theta_i)L = M_d L$, where θ_i is the initial moisture content, θ_s is the saturated moisture content, and $M_d = \theta_s - \theta_i$ the initial moisture deficit.

Darcy's law is then applied as an approximation to the saturated conditions between the soil surface and the wetting front, as indicated in Figure 9.6b (Bedient and Huber, 1992).

The volume of infiltration down to the depth L is given by

$$F = L(\theta_s - \theta_i) = LM_d \tag{9.10}$$

Neglecting the depth of ponding at the surface, the original form of the Green-Ampt equation

$$\begin{aligned} f &= K_s[1 - (\theta_s - \theta_i)\psi_f / F] \\ &= K_s[1 - M_d \psi_f / F] \end{aligned} \tag{9.11}$$

Because ψ_f is negative, Eq. (9.11) indicates that the infiltration rate is a value greater than the saturated hydraulic conductivity, as long as there is sufficient water at the surface for infiltration, as sketched in curves C and D of Figure 9.6c. Functionally, the infiltration rate decreases as the cumulative infiltration increases.

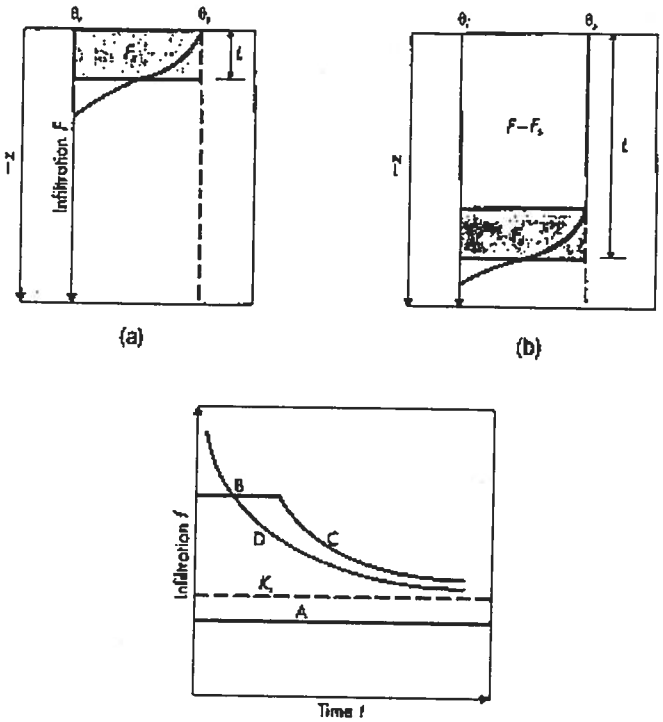

Figure 9.6 Moisture and infiltration relations. (a) Moisture profile at moment of surface saturation. (b) Moisture profile at later time. (c) Infiltration behavior under rainfall. Source: Mein and Larson, 1973.

The rainfall intensity, i, is often less than the potential infiltration rate given by Eq. (9.11), in which case $f = i$. Let the corresponding volume of infiltration be F_s. With $f = i$, Eq. (9.11) can then be solved for F_s, the volume of infiltration at the time of surface saturation (t_s, the time at which Eq. (9.11) becomes valid),

$$F_s = [(\theta_s - \theta_i)\psi_f]/[1 - i/K_s] = M_d\psi_f/(1 - i/K_s) \qquad (9.12)$$

We require $i > K_s$ in Eq. (9.12) and remember that ψ_f is negative. The Green-Ampt infiltration prediction is thus the following:

If $i \le K_s$, then $f = i$ (curve A in Figure 9.6c)
If $i > K_s$, then $f = i$ until $F = it_s = F_s$ (Eq. (9.12)
After the surface is saturated, the following is used, $f = K_s[1 - M_d\psi_f/F]$ (Eq. (9.11)) for $i > K_s$ and $f = i$ for $i \le K_s$.

The combined process is sketched in curves B and C of Figure 9.6c. As long as the rainfall intensity is greater than the saturated hydraulic conductivity, the infiltration rate asymptotically approaches K_s, as a limiting lower value. Mein and Larson (1973) found excellent agreement when using the Green-Ampt method, numerical solutions of Richard's equation, and experimental soils data. If the rainfall rate starts above K_s, drops below it, and then rises back above it during the infiltration computation, the use of Green-Ampt becomes more complicated, making it necessary to redistribute the moisture in the soil column rather than maintaining the assumption of saturation from the surface down to the wetting front shown in Figure 9.6b. The use of the Green-Ampt procedures for unsteady rainfall sequences is illustrated by Skaggs and Khaleel (1982).

Equation (9.11) predicts infiltration rate, f, as a function of cumulative infiltration, F, not time. Because $f = \partial F/\partial t$, the equation can be converted into a differential equation, the solution of which can be solved iteratively for $F(t)$ (Chow et al., 1988). Then Eq. (9.11) can be used to determine $f(t)$.

A major advantage of the Green-Ampt model is that, in principle, the necessary parameters, K_s, ψ_f, and $M_d = \theta_s - \theta_i$, can be determined from physical measurements in the soil, rather than empirically as for the Horton parameters. For example, saturated hydraulic conductivity (often loosely called permeability) is tabulated by the U.S. Soil Conservation Service (SCS) for a large number of soils as part of that agency's Soil Properties and Interpretation sheets (available from local SCS offices). An increasing quantity of tension versus moisture content data (of the type shown in Figure 9.2) are also available, from which a value of ψ_f can be obtained by integration over the moisture content of interest. For example, several volumes of such information have been assembled for Florida soils (e.g., Carlisle et al., 1981). In practice, the Green-Ampt parameters are often calibrated, especially when used in continuous simulation models.

A useful source of information on Green-Ampt parameters is provided by Rawls et al. (1983), who present data for a large selection of soils from across the United States. These data are shown in Table 9.1. Two porosity values are given: total and effective. Effective porosity accounts for trapped air and is the more reasonable value to use in computations. It can be seen in Table 9.1 that as the soil particles get finer, from sands to clays, the saturated hydraulic conductivity, K_s, decreases, the average wetting front suction, ψ_f, increases (negatively), and porosity, θ_s, is variable. Table 9.1 provides valuable estimates for Green-Ampt parameters, but local data (e.g., Carlisle et al., 1981) are preferable if available. Missing is the initial moisture content, θ_i, since it depends on antecedent rainfall and moisture condi-

TABLE 9.1 Green-Ampt infiltration parameters for various soil texture classes

Soil Class	Porosity η	Effective Porosity θ_E	Wetting Front Soil Suction Head ψ (cm)	Hydraulic Conductivity K(cm/hr)	Sample Size
Sand	0.437 (0.374-0.500)	0.417 (0.354-0.480)	4.95 (0.97-25.36)	11.78	762
Loamy sand	0.437 (0.363-0.506)	0.401 (0.329-0.473)	6.13 (1.35-27.94)	2.99	338
Sandy loam	0.453 (0.351-0.555)	0.412 (0.283-0.541)	11.01 (2.67-45.47)	1.09	666
Loam	0.463 (0.375-0.551)	0.434 (0.334-0.534)	8.89 (1.33-59.38)	0.34	383
Silt loam	0.501 (0.420-0.582)	0.486 (0.394-0.578)	16.68 (2.92-95.39)	0.65	1206
Sandy clay loam	0.398 (0.332-0.464)	0.330 (0.235-0.425)	21.85 (4.42-108.0)	0.15	498
Clay loam	0.464 (0.409-0.519)	0.309 (0.279-0.501)	20.88 (4.79-91.10)	0.10	366
Silty clay loam	0.471 (0.418-0.524)	0.432 (0.347-0.517)	27.30 (5.67-131.50)	0.10	689
Sandy clay	0.430 (0.370-0.490)	0.321 (0.207-0.435)	23.90 (4.08-140.2)	0.06	45
Silty clay	0.479 (0.425-0.533)	0.423 (0.334-0.512)	29.22 (6.13-139.4)	0.05	127
Clay	0.475 (0.427-0.523)	0.385 (0.269-0.501)	31.63 (6.39-156.5)	0.03	291

The numbers in parentheses below each parameter are one standard deviation around the parameter value given.
Source: Rawls, Brakensiek, and Miller, 1983.

tions. Typical values for $M_d = \theta_s - \theta_i$, are given in the SCS Soil Properties and Interpretation sheets and are usually termed "available water (or moisture) capacity, in./in." Values usually range from 0.03 to 0.30. The value to use for a particular soil in question must be determined from a soil test. Otherwise, a conservative (low) M_d value could be used for design purposes (e.g., 0.10).

Example 9.1 GREEN-AMPT TIME TO SURFACE SATURATION
Guelph Loam has the following soil properties (Mein and Larson, 1973) for use in the Green-Ampt equation:

$K_s = 3.67 \times 10^{-4}$ cm/sec
$\theta_s = 0.523$
$\psi = -31.4$ cm water

For an initial moisture content of $\theta_i = 0.3$, compute the time to surface saturation for the following storm rainfall:

$i = 6K_s$ for 10 min
$i = 3K_s$ thereafter

Solution. The initial moisture deficit, $M_d = 0.523 - 0.300 = 0.223$. For the first rainfall segment, we compute the volume of infiltration required to produce saturation from Eq. (9.12):

$$F_s = \psi_f M_d / (1 - i/K_s) = (-31.4 \text{ cm})(0.223) / (1 - 6K_s/\text{Ks}) = 1.40 \text{ cm}$$

The rainfall volume during the first 10 minutes is

$$10i = (10 \text{ min})\,(6 \cdot 3.67 \_ 10\text{-}4 \text{ cm/sec})(60 \text{ sec/min}) = 1.31 \text{ cm}$$

since 1.31 < 1.40, all rainfall infiltrates and surface saturation is not reached, and F(10min) = 1.31 cm.

The volume required for surface saturation during the lower rainfall rate of i = 3Ks is

$$\text{Fs} = (-31.4 \text{ cm})(0.223) / (1 - 3\text{Ks} / \text{Ks}) = 3.50 \text{ cm}$$

Thus, an incremental volume of $\Delta F = \text{Fs} - \text{F(10 min)} = 3.50 - 1.31 = 2.19$ cm must be supplied before surface saturation occurs. This requires an incremental time of

$$\Delta t = \Delta F/i = (2.19 \text{ cm}) / (3 \cdot 3.67 \times 10^{-4} \text{ cm/sec}) = 1989 \text{ sec}$$
$$= 33.15 \text{ min}$$

Thus, the total time to surface saturation is 10 + 33.15 = 43.15 min.

9.7 TRANSPORT PROCESSES IN THE UNSATURATED ZONE

The movement of contaminants in the vadose zone is an important hydrologic problem. The unsaturated zone, the region bounded at its top by the soil surface and below by the ground water table, represents the conduit through which liquid and gaseous constituents can be attenuated and transformed. Surface and ground waters are linked by the unsaturated zone, which is recognized as a key factor in the improvement and protection of the quality of ground water supplies.

The three major environmental health and safety problems that result from gasoline spills to the subsurface are: soil contamination, ground water contamination, and fire and explosion hazards (Hoag and Marley, 1986). In reality, transport in the unsaturated zone is much more complex than in the saturated zone mainly because there are numerous phases of interest: soil, water, air, and contaminant. Chemicals exist in the unsaturated zone in four phases: dissolved in soil moisture, sorbed to the soil particles, as nonaqueous phase liquids (NAPL), and as an envelope of organic vapors. As time goes by, the immiscible liquid migrates downwards leaving behind blobs of material trapped by capillary forces in the pores, often referred to as the residual phase. If the spilled product is less dense than water, it accumulates on top of the water table forming a light nonaqueous phase liquid (LNAPL) pool.

Figure 9.7 shows NAPL migration in the subsurface. The free product can be recovered by bailing or skimming. Unfortunately, after the source has been removed, the threat posed from the residual phase still persists as the sorbed and the retained materials serve as a constant reservoir of contamination to the underlying aquifers and overlying ground surface. Ground water contamination from the residual phase that exists in the vadose zone has been an issue of major concern. The parameters of interest in this case are: the travel time from the ground surface to the water table, the amount of contaminant that actually reaches the water table, and the rate at which it enters the ground water aquifer.

Organic vapors have been identified as one of the more ubiquitous groups of hazardous chemicals present in contaminated soils and ground water. They can migrate much faster than the liquid phase. Moreover, the vapor flow velocities and direction are not controlled by ground water gradients. Volatilization from residual NAPL or from NAPL dissolved in water results in the formation of a vapor plume, which can spread by vapor diffusion, and by density induced advection of the soil gas mixture. As it spreads, the vapor plume also contaminates the soil moisture and soil matrix as a result of phase partitioning. Vapors less dense than air may rise to the ground surface where they become a potential for inhalation or explosion if they get into the basement of structures (Sleep and Sykes, 1989). On the other hand, ground water contamination can occur due to vapor migration downwards towards the capillary fringe, due to a rise in the water table, and due to recharge by infiltration.

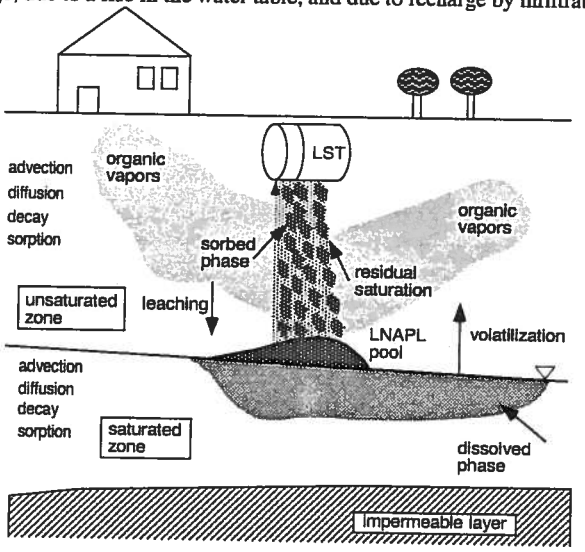

Figure 9.7 Contamination migration pathways in the unsaturated zone.

9.7.1 Volatile Emissions from Soil

Investigations of fate and transport of chemicals in the unsaturated zone must inherently deal with multiphase issues. Contaminants exist in four phases: aqueous, soil, vapor, and immiscible oil phases. The pore space is filled by the sum of the fluids present so that porosity equals the sum of the volumetric fluid contents. The concentrations of a constituent in the aqueous, vapor, and oil phases are designated C_a, C_v, and C_o, all on a mass per unit volume basis. The chemical soil phase concentration is designated as mass of chemical sorbed per unit mass of soil, C_s. The total concentration is specified by C_T.

The modeling of emissions to the atmosphere from soil processes has been dealt with by Jury et al. (1983) and Enfield et al. (1985). Jury et al. (1983) assume that: (1) the chemical of total concentration C_{Ti} is incorporated uniformly to a specified depth, L; (2) volatilization of the chemical takes place through a stagnant air layer just above the soil surface; (3) there is a steady flux of water through the soil; and (4) there is an infinite depth of uniform soil below the zone of incorporation. The boundary conditions considered by Jury et al. (1983) are as follows:

$$C_T = C_{T_i}, \qquad 0 < X < L \quad \text{for} \quad t = 0 \tag{9.13}$$

$$C_T = 0, \qquad X > L \quad \text{for} \quad t = 0 \tag{9.14}$$

The transport of the chemical through the stagnant boundary is equal to the flux at the soil surface such that:

$$-D_E \frac{\partial C_T}{\partial X} + V_E C_T = -H_E C_T \quad \text{for } X = 0 \text{ at all } t \tag{9.15}$$

where D_E, V_E are the effective dispersion coefficient, effective velocity, and H_E is the effective mass transfer coefficient defined by:

$$H_E = \frac{h}{B_v} \tag{9.16}$$

where h is the mass transfer coefficient across the stagnant air film, and B_v is defined by:

$$B_v = \left[\frac{\theta}{H} + \theta_o \frac{K^{o-w}}{H} + \theta_a + \rho \frac{K_d}{H}\right] \tag{9.17}$$

where θ is the volumetric water content, ρ is the density of the soil phase, θ_o is the volumetric oil content, θ_a is the volumetric vapor content, K_d is the soil water partitioning coefficient, H is the Henry's Law constant, and K^{o-w} is the oil-water partitioning coefficient.

The vapor flux at the surface of the soil is estimated using:

$$J(0,t) = -H_E C_T \tag{9.18}$$

Jury et al. (1983) solved the appropriate equations analytically and obtained an expression for the vapor flux of organics from soils.

Thibodeaux and Hwang (1982) have also presented solutions for estimating volatile emissions from land treatment. Their approach (illustrated in Figure 9.8) assumes that there is no movement of liquids in the soil, and that no adsorption or biodegradation takes place. It is assumed that the soil is contaminated between depths h_s and h_p. As the contaminant evaporates and the vapor diffuses upward to the surface, a "dried-out" zone develops. The flux through the surface (ignoring mass transfer through the stagnant boundary layer above the soil) is given by:

$$J(0,t) = -\frac{D_V C_{WZ}}{h_p - y} \tag{9.19}$$

where D_V is the effective diffusivity in the air-filled pores and C_{WZ} is the vapor phase concentration of the contaminant in the wet zone.

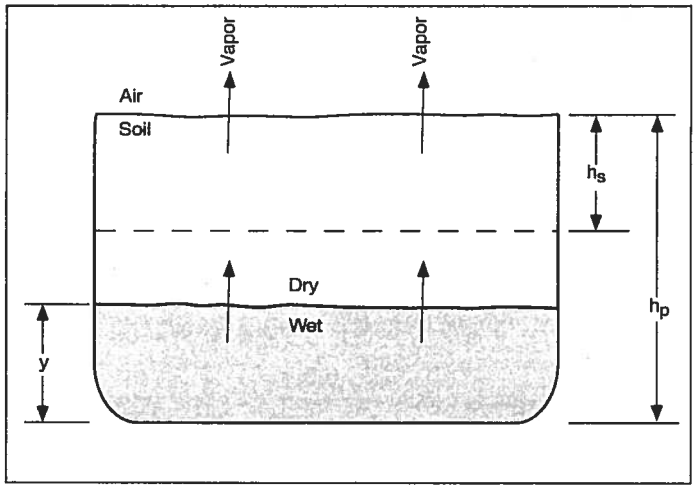

Figure 9.8 Thibodeaux-Hwang land treatment volatilization model. Source: Short, 1986.

A mass balance on the system using the appropriate boundary conditions yields an expression for the flux through the wet-dry interface:

$$J(0,t) = D_V C_{WZ} \sqrt{h_s^2 + 2(h_p - h_s) D_V C_{WZ} A t M_A} \tag{9.20}$$

where M_A is the mass of contaminant applied, and A is the soil surface area over which the contaminant is applied.

9.7.2 Soil Gas Investigation

Recently sampling and analysis of soil gas for delineation of subsurface volatile organic compounds (VOCs) has become very popular. The presence of VOCs in soil gas indicates that volatile organics may be present either in the vadose zone or in the saturated zone. Therefore, soil gas surveys are often applied to define the areal extent of contamination from a source in the vadose zone or to identify ground water contamination problems. The data obtained from these surveys are used for locating soil borings and monitoring wells, which are required to delineate the distribution of subsurface contamination (Pankow and Cherry, 1996).

Good detection of vapors is common in shallow ground water settings and fairly permeable soils. Compounds that are more suitable for detection are those that have a boiling point less than 150 °C, low aqueous solubility, and vapor pressure higher than 10 mm Hg at 20 °C.

Soil gas samples may be collected by pumping a sample from the vadose zone, which can be analyzed in the field and actual concentrations are measured (Figure 9.9). This method may disturb the vapor distribution due to sample withdrawal. Another method of sampling is by burying an absorbent material within the vadose zone and capturing the VOCs by sorption. The disadvantage of this method is that it measures relative concentrations and not absolute concentrations at the different locations. Several methods currently being used for the analysis of soil gas samples are listed in Table 9.2.

TABLE 9.2 Methods of Sampling for VOCs

Method	Usage
Electron capture detector (ECD)	Sensitive to halocarbon compounds such as TCE, PCE, TCA
Flame ionization detector (FID)	Sensitive to hydrocarbon compounds
Photoionization detector (PID)	Sensitive to vinyl chloride
Hall electrolytic conductivity detector	Sensitive to most halogenated compounds

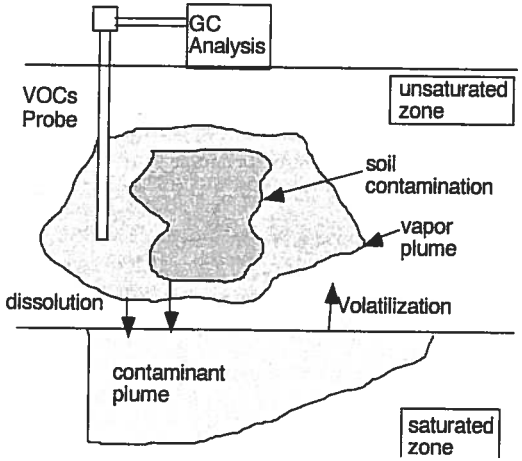

Figure 9.9 Soil gas sampling.

9.8 GOVERNING EQUATIONS FOR VAPOR TRANSPORT

Vapor flow and transport in porous media may occur in response to pressure and concentration gradients (Massmann, 1989). Pressure gradients may arise from: barometric pressure fluctuations (Massmann and Farrier, 1992); vaporization of a liquid (Baehr and Bruell, 1990; Mendoza and Frind, 1990a); water table fluctuations (McCarthy and Johnson, 1993); or density gradients (Falta et al., 1989; Sleep and Sykes, 1989). Volatile compounds with high molecular weights result in higher vapor densities that drive advective flows. Transport may also arise from induced advective flows created by applying vacuum as in soil vapor extraction (SVE) systems. In case of negligible pressure gradients, transport is dominated by concentration gradients (diffusion). Pressure gradients due to barometric fluctuations can be neglected at small pressure variations (up to 10 mbar) (Conant et al., 1996). Sensitivity analyses conducted by Mendoza and Frind (1990), have demonstrated that advective fluxes caused by vaporization of organic compounds are of minor importance compared to density-driven advection. Mechanical dispersion and molecular diffusion play a big role in spreading contaminants in the gas phase. Air diffusion coefficients for organic compounds are several orders of magnitude larger than aqueous diffusion coefficients; therefore, molecular diffusion is usually more dominant than mechanical dispersion in vapor movement, except for areas close to venting wells in SVE systems where vapor velocities are very high (Benson et al., 1993).

9.8.1 Flow Equation

The similarity between air and water flow has resulted in modifying ground water flow equations to represent gas flows. The major differences that exist between water and gas flow are as follows (Brusseau, 1991):

1. Water is incompressible whereas gas is compressible, that is, gas density is dependent on pressure, which results in a nonlinear flow equation. Gas compressibility can be neglected where the pressure difference inducing gas flow is less than 20%. Almost all soil venting systems operate under these conditions, and the incompressibility assumption is valid.
2. Slip flow for water is negligible, whereas nonzero gas fluxes at pore walls are not negligible. Slip flows are not observed when the pressure difference is less than 20%, and can be excluded from the modeling process for gas transport in venting systems.
3. Water flow in porous media is laminar and Darcy's law is applicable. Darcy's law does not describe gas flow since small pressure gradients usually generate significant gas flows. Laminar flow may not be valid under these conditions. However, conditions under which gas compressibility and slip flows are negligible would be appropriate for using Darcy's law.

Equations of fluid flow in porous media are obtained by combining the mass continuity equation with Darcy's Law which yields the following 3-D air flow equation (Bear, 1979):

$$\frac{\partial}{\partial x}\left(k_{gxx}\frac{\partial \phi}{\partial x}\right)+\frac{\partial}{\partial y}\left(k_{gyy}\frac{\partial \phi}{\partial y}\right)+\frac{\partial}{\partial z}\left(k_{gzz}\frac{\partial \phi}{\partial z}\right)=S_g\frac{\partial \phi}{\partial t} \tag{9.21}$$

$$\phi = P_g^2 \tag{9.22}$$

where x,y,z are Cartesian coordinates aligned along the major axes of the effective air permeability tensor with diagonal components k_{gxx}, k_{gyy}, k_{gzz}. S_g is the pneumatic equivalent of specific storage [L^{-1}], and P_g is the gas/vapor pressure [M/LT^2]. P_g^2 is substituted by ϕ for linearization of the equation.

The differential equation governing air flow is nonlinear because air density increases with air pressure. However, if the difference in air pressure within flow fields does not exceed 0.2 atm, which is common to natural and soil vapor extraction systems, the linear ground water flow equation may be used to simulate air flow (Massman, 1989).

The flow equation may be solved numerically by finite difference or finite element techniques (Anderson and Woessner, 1992). Alternatively, the flow equation may be simplified and solved analytically as described by Johnson (1991).

9.8.2 Organic Vapor Transport

The vapor phase transport of mass has much in common with the transport of dissolved contaminants in ground water. The processes of advection and dispersion operate to physically transport the mass, while the chemical processes are involved with the generation of the contaminants through volatilization and subsequent interactions with the water and solid phases in the system.

Removal of mass from a spill depends upon the process of volatilization, which is a phase partitioning between a liquid and a gas. For solvents, the process is described in terms of equilibrium theory by a form of Raoult's law,

$$P_i = x_i \gamma_i P_i^0 \tag{9.23}$$

where P_i is the vapor pressure of component i (atm) in the soil gas, x_i is the mole fraction of the component in the solvent, and P_i^0 is the vapor pressure of the pure solvent at the temperature of interest; these are tabulated constants (e.g., Verschueren, 1983). An activity coefficient γ_i for the i^{th} component in the mixture is added to account for nonidealities (Hinchee et al., 1986). By applying the ideal gas equation, the partial pressures calculated in Eq. (9.23) can be expressed in terms of concentration:

$$C_{s,i} = \frac{P_i MW_i}{RT} \tag{9.24}$$

where $C_{s,i}$ is the saturation concentration of compound i [mg/cm^3], T is temperature [K], R is the universal gas constant [82.04 atm·cm^3·mole^{-1}·K^{-1}], MW_i is the molecular weight of compound i [mg/mole], and P_i is the partial pressure of the compound i [atm].

The equilibrium approach applies in cases where the rate of volatilization is large relative to the rate of physical transport through the medium. Where the flow of air contacts residual product in every pore, phase equilibrium is achieved quite rapidly at least for the more volatile compounds at the start of venting. One important reason for less than equilibrium concentrations of vapor is geologic heterogeneities that cause some of the air flow to avoid most of the contaminated zones.

With spills of complex solvent mixtures like gasoline, soil venting removes the components with higher vapor pressure first. The residual contamination, thus, becomes progressively enriched in the less volatile compounds. Because of this compositional change, the overall rate of mass removal decreases with time. This process has been described mathematically by Marley and Hoag (1984) and Johnson (1991) using forms of Eq. (9.24) and information on the most volatile components of gasoline.

Vapor pressures for organic compounds increase significantly as a function of increasing temperature. For example, the vapor pressure for a volatile compound like benzene increases from 0.037 atm at 32 °F to 0.137 atm at 80 °F (Johnson et al., 1988; Johnson, 1991). Over the same temperature range, the vapor pressure for n-dodecane increases from

2.8×10^{-5} atm to 2.3×10^{-4} atm. The main implication of this result is that the overall time required for cleanup will change depending upon temperature.

The physical transport process, advection and dispersion, play an important role with respect to vapor transport. The simplest and most extensively analyzed model of physical transport assumes that advection transports contaminants from the point of generation to the vapor extraction well (Figure 9.10a), that the distribution of contaminants would be reasonably homogeneous, and that much of the air flow would have the opportunity to move through the bulk of the spill. Ideally, the vapor concentration in the fraction of air moving through the spill is the equilibrium concentration determined by Raoult's law. In Figure 9.10a, about 25% of the air passes through the spill giving a vapor concentration in the well

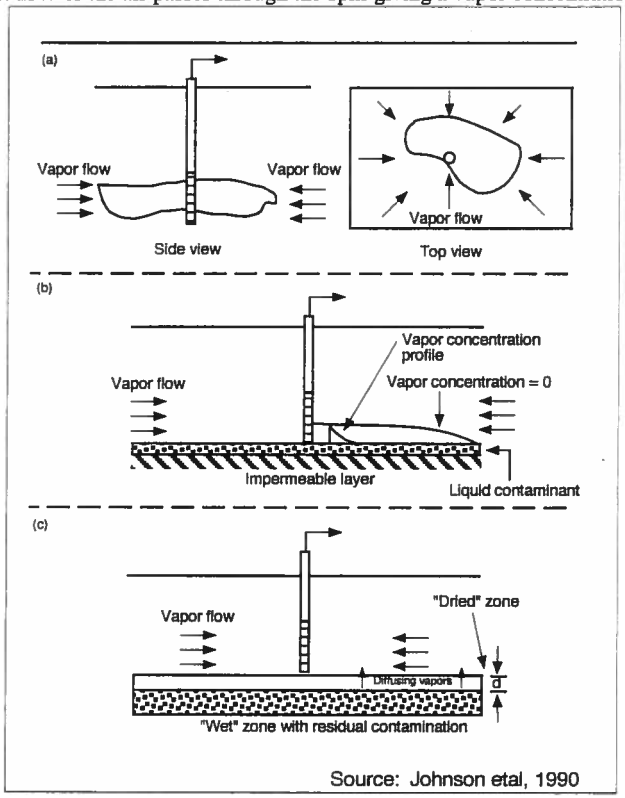

Figure 9.10 Different ways in which the circulating air interacts with a volatile contaminant source.

that is 25% of equilibrium value and a removal rate of $0.25QC_s$, where Q is the airflow, C_s is the equilibrium concentration.

However, in heterogeneous media or when pure product is present, the air flow may not pass directly through the spill. Specific examples cited by Johnson et al. (1988, 1990) include: (1) air flow across the surface of a free-liquid floating on the water table or low permeability layer (Figure 9.10b), or (2) product trapped in a lower permeability lens (Figure 9.10c). In both of these cases, the mass loss rate of contaminants is controlled by the rate at which mass can diffuse into the moving vapor stream. Thus, when flowing air bypasses the spill, the rate of mass removal may be much lower than for the homogeneous case. The result may be a vapor extraction system that circulates considerable quantities of air without removing much of the contaminant. Mathematical approaches for estimating the contaminant removal rates under these more complex conditions are presented by Johnson et al. (1990).

9.8.3 Transport Equations

The primary mechanisms involved in contaminant transport in porous media are: advection, diffusion, dispersion, and reactions as previously described in chapter 6. The general mass balance equation for each chemical component i in each fluid phase α is: (Rathfelder et al., 1991):

$$\frac{\partial}{\partial t}\left(nS_\alpha C_{\alpha i}\right) = -\nabla \cdot nS_\alpha\left(C_{\alpha i}V_{m\alpha} + J^d_{\alpha i} + J^m_{\alpha i}\right) + nS_\alpha C_\alpha \Gamma_{\alpha i} - I^i_{\alpha\beta} \tag{9.25}$$

subject to

$$\sum_{i=1}^{N_\alpha} C_{\alpha i} = C_\alpha \tag{9.26}$$

where S_α is the fluid saturation [dimensionless], $C_{\alpha i}$ is the component concentration in each phase [M/L^3], $C_{\alpha i}V_{m\alpha}$, $J^d_{\alpha i}$, and $J^m_{\alpha i}$ are the component mass flux in each phase by advection, dispersion and diffusion [M/L^{2}T] respectively, $\Gamma_{\alpha i}$ is the rate of component mass production/removal by pumping/injection or reactions per unit mass of each phase [1/T], $I^i_{\alpha\beta}$ is the interphase mass transfer [M/L^{3}T] between adjacent phases, α and β. A similar equation is expressed for the solid phase by replacing the concentration terms with $\rho_b C_{si}$, where ρ_b is the soil bulk density [M/L^3], and C_{si} is the component concentration in the solid phase [M/M]. Equation (9.26) states that the sum of component concentrations in each phase is equal to the density of the phase. N_α represents the number of components.

Advective fluxes follow Darcy's law

$$nS_\alpha V_{m\alpha} = \frac{kk_{r\alpha}}{\mu_\alpha}\nabla P_\alpha = \bar{V}_\alpha \tag{9.27}$$

where k is the intrinsic permeability tensor [L^2], and $k_{r\alpha}$ is the fluid relative permeability [dimensionless], μ_α is the fluid viscosity [M/LT], P_α is the fluid pressure [M/LT^2], and $\bar{V}_\alpha$ is the fluid specific discharge vector [L/T].

Dispersive fluxes follow Fick's law

$$J^d_{\alpha i} + J^m_{\alpha i} = -D_{\alpha i}\cdot\nabla C_{\alpha i} \tag{9.28}$$

where $D_{\alpha i}$ is the dispersion tensor for each component in each phase [L^2/T], which is evaluated by the following expression (Bear, 1979):

$$(D_{\alpha i})_{ij} = \alpha_T \bar{V}\delta_{ij} + (\alpha_L - \alpha_T)\bar{V}_i\bar{V}_j / \bar{V} + D^*_{\alpha i}\delta_{ij} \tag{9.29}$$

where $i,j = x,y,z$, α_L and α_T, are the longitudinal and transverse dispersivity of the porous media respectively [L], $\bar{V}$ is the average velocity, δ_{ij} is the Kronecker Delta [dimensionless], and $D^*_{\alpha i}$ is the effective molecular diffusion coefficient for each component in each phase [L^2/T]. If advective flows are high, then the first two terms in Eq. (9.29) will be more dominant than the diffusion term. More often, if advective fluxes are negligible, the dispersion coefficient will be a function of the air diffusion coefficient, and the transport equation reduces to Fick's Law.

As moisture contents vary in the vadose zone, the pore space available for vapor and water diffusion is reduced, and the transport pathways become more convoluted. Thus, the molecular diffusion coefficient is calculated using the Millington and Quirk (1961) relationship to account for tortuosity (Mendoza and Frind, 1990a):

$$D^*_{\alpha i} = \frac{\theta_\alpha^{10/3}}{n^2} D_{\alpha i} \tag{9.30}$$

where $D^*_{\alpha i}$ is the effective molecular diffusion coefficient for each component in each phase [L^2/T], θ_α is the porosity filled by each phase [L^3/L^3], $D_{\alpha i}$ is the component diffusion coefficient at each phase [L^2/T]. Air diffusion coefficients for organic compounds are much larger than aqueous diffusion coefficients. Therefore, diffusion is generally more significant in gas transport than in ground water systems. The free air diffusion coefficient is temperature dependent. However, this phenomenon is usually neglected since it was observed that a 10 °C increase in the temperature of the unsaturated zone results in a 6% increase of the diffusion coefficient (Conant et al., 1996).

Many investigators have considered vapor transport in the gas phase and water phases, since the NAPL phase is immobile in the unsaturated zone (Sleep and Sykes, 1989). The interphase mass transfer terms in the water transport equation represent vapor-water partitioning, desorption from the solid phase, and dissolution from the NAPL phase. The interphase mass transfer terms in the gas/vapor transport equation represent vapor-water partitioning and volatilization from the NAPL phase. The transport equations for the vapor and water phases are linked by the vapor-water partitioning terms. In many instances, the reaction term is neglected in order to assume the worst case condition, that is, no biodegradation or transformation is assumed to occur. Some investigators have considered transport in the gas phase only assuming that soil moisture is usually below or at residual saturation, and may not be affected by the mobile vapor phase in the unsaturated zone.

9.8.4 Equilibrium Partitioning

Equilibrium partitioning between phases is in many cases a valid assumption. The equilibrium form is valid in diffusion-dominated or weakly advective environments. In these cases, it is assumed that chemical equilibrium exists between the contaminant concentrations in the different phases, and that interphase mass transfer is not rate-limited, that is phase transfer is instantaneous. The linear relationships between contaminant concentrations in different phases allow for expressing the advection-dispersion equation in terms of an individual phase concentration (Rathfelder et al., 1991). Although linear isotherm equations are usually satisfactory for describing water-soil equilibrium, nonlinear isotherms can better represent many organic and inorganic chemicals (Brusseau, 1994). The transport equations are summed over all phases, eliminating all interphase terms and a retardation coefficient determines the delay in vapor movement due to phase partitioning or sorption processes.

9.8.5 Non-Equilibrium Partitioning

Under strongly advective conditions, such as in SVE systems, equilibrium partitioning is not always suitable since it does not reproduce the tailing phenomenon that is observed in experimental studies (Armstrong et al., 1994). Tailing occurs when venting systems are restarted after shutdown, and has been attributed to the rate-limited interphase mass transfer processes. Moreover, equilibrium partitioning may dominate while contaminants are present in a NAPL form, but not for dilute solutions. Following removal of NAPL, VOC transfer to the gas phase occurs by desorption from the solid phase into the pore water, then through volatilization from pore water into the gas phase. Rate limited mass transfer controls these stages (Rathfelder et al., 1995). Rate limiting processes may be generated by: (1) rate limited mass transport between phases including film transfer limitations and intraaggregate diffusional processes (Brusseau, 1991; Gierke et al., 1990); (2) physical by passing of the contaminated region due to low permeability; (3) aquifer heterogeneity (Ho and Udell, 1992); (4) non-equilibrium adsorption/desorption (Brusseau, 1991).

Mass transfer processes at the interface of two adjacent phases may be visualized as a series of steps: (1) advection/diffusion in the bulk phase of one fluid towards the interface, (2) accumulation, advection/diffusion, reaction, and sorption/desorption at the interface, (3) advection/diffusion away from the interface in the bulk phase of the other fluid (Powers et al., 1991). Mass transfer limited processes are modeled by incorporating first-order kinetic expressions into the interphase terms of the transport equation, whereby the mass transfer driving force is proportional to the difference between equilibrium and actual concentrations.

9.9 VADOSE ZONE FLOW AND TRANSPORT MODELS

Mathematical models have become an important tool in predicting vapor excursion distances and directions which help in evaluating vapor control alternatives. A vapor transport model can greatly assist in the correlation of vapor phase to ground water aqueous phase concentrations, in designing and evaluating the performance of SVE systems, and in evaluating the long term hazards associated with the problem and the system response to alternative remedial measures (Metcalfe and Farquhar, 1987, Benson et al., 1993, Jordan et al., 1995, Rathfelder et al., 1995). A number of mathematical models have been presented in the literature for the description of multiphase flow and transport in the vadose zone. These vary greatly in level of complexity and in the processes they describe (Rathfelder et al., 1995).

9.9.1 Types of Models

Screening models are rather simple and require limited site data; thus, they can be used to make preliminary determinations of the extent of contamination and the feasibility of SVE systems as a method of remediation at contaminated sites. Screening models such as Hypervent (Johnson, 1991) can aid in determining site permeability, extraction well radius of influence and flow rate and mass removals using analytical, semi-analytical or numerical solutions that may be subject to fairly limiting assumptions such as a homogeneous subsurface and a single extraction well. The initial determination of whether SVE is potentially feasible for a site should be with a screening tool.

Numerical air flow models can accommodate complex geologic and boundary conditions. They can allow representation of two and three dimensions in space rather than the 1-D axisymmetric domain represented by most screening tools. For more detailed analysis of contaminant migration and design of SVE systems, models such as AIRFLOW/ SVE (see Table 9.3) may provide quantitative flow analysis of soil gas pressure, flow rates, extraction well placement, extraction rates and air flow patterns.

A more accurate description of vapor movement may also be provided by vapor flow and transport models (compositional models) such as VENT3D (Benson et al., 1993; Benson, 1994), which can simulate the physical and chemical processes that govern vapor movement in the subsurface. The advantage of using these models is that they can estimate the air flow regime and the movement or removal of contaminants by SVE. They may also be used to design and evaluate the effectiveness of SVE systems, and to estimate contaminant removals and the effect of mass transfer limitations and soil heterogeneities on system

TABLE 9.3 Selected Models for Unsaturated Zone Analysis

Model Name	Model Description	Model Processes
	SCREENING MODELS	
HyperVentilate (1991) Paul C. Johnson. Available from EPA	A screening model that can be used to determine the potential feasibility of SVE for remediation at contaminated sites. The flow equation is solved analytically. The transient one-dimensional multicomponent contaminant transport equation is solved by finite difference.	Steady-state, radial, confined air flow to a vapor extraction well. Transient, mass balance approach, volatilization based on Raoult's Law.
BioSVE (1998) Scientific Software Group. Washington, D. C.	A screening model based on Johnson's model Hypervent (1991) that evaluates different remediation schemes such as SVE, Vacuum Enhanced Recovery and Bioventing. Models recovery versus time of up to 250 components partitioned between water, vapor, NAPL and soil.	Equilibrium partitioning between phases is assumed. Nonequilibrium partitioning may be incorporated using an efficiency factor. Oxygen limited biodegradation based on instantaneous reaction. Kinetics effects handled using a bio-efficiency factor. Can simulate recovery of the free floating product along with bioventing the unsaturated zone.
	AIR FLOW MODELS	
MODAIR (1996) **P3DAIR (1989)** Guo Zheng Scientific Software Group, Washington , D. C.	MODAIR simulates airflow based on MODFLOW, the groundwater code. P3DAIR simulates the advective movement of vapors in the unsaturated zone. It is a particle tracking program for calculating air flow paths and travel times. The two models are used together for SVE system design.	Air flow and pressure calculations are computed by MODAIR. Vapor extraction wells can be specified as pressure controlled or volumetric rate controlled. P3DAIR calculates the travel times and pathlines for each particle along the x,y, and z coordinates and initial and final positions of particles captured by sources/sinks. It can be used in 2-D or 3-D, steady-state or transient.
	MULTIPHASE MODELS	
T2VOC (1995) R. W. Falta Karsten Pruess Stefan Finsterle Alfredo Battistelli	Three-dimensional, finite difference model for simulating flow and transport of organic contaminants in non-isothermal, heterogeneous, multi-phase systems.	Flow and transport of air, water and a VOC are simulated. Interphase mass transfer include evaporation and boiling of NAPL, dissolution of NAPL into the aqueous phase, condensation of VOC into the NAPL, equilibrium partitioning between the gas, aqueous, and NAPL phases, evaporation and boiling of the aqueous phase, and condensation of water vapor from the gas phase. Accounts for heat transfer due to conduction, multiphase convection, and gaseous diffusion.
Bioventing (1997) Environmental Systems and Technologies, Inc. Blacksburg, VA.	Finite difference, one dimensional, multiphase, multicomponent model for evaluation of design options for air-based in situ remedial technologies.	Air flow rates are calculated. Contaminant composition and recovery versus time is calculated. The model considers leakage from the ground surface, equilibrium partitioning, oxygen-limited biodecay, air turnover rates and their effect on recovery. The model computes costs for design options.

TABLE 9.3 Selected Models for Unsaturated Zone Analysis (Continued)

Model Name	Model Description	Model Processes
	FLOW AND TRANSPORT MODELS IN UNSATURATED/SATURATED ZONE	
FEMWATER/ FECWATER (1987) Yeh, G. T. Ward, D. S.	Two-dimensional finite element model to simulate transient cross-sectional flow in saturated / unsaturated, anisotropic, heterogeneous porous media	Capillary action, infiltration, ponding
VAM3D (1988) Huyakorn, P. S.	Three-dimensional finite element model that simulates flow and transport in variably saturated porous media	Advection, dispersion, adsorption and degradation
Chemflo (1989) Nofziger, D. L. Scientific Software Group, Washington, D. C.	One-dimensional, finite difference model that simulates the movement of water and chemicals in unsaturated soils.	Water movement is modeled using Richard's equation, and contaminant transport using the convection-dispersion equation. Partitioning is instantaneous and reversible.
AIRFLOW/SVE (1993) Waterloo Hydrogeologic Software, Ontario, Canada.	Three-phase, finite difference model for simulating vapor flow and transport of multicomponent mixtures in heterogeneous, anisotropic soils.	Steady-state, radial, symmetric vapor flow and transport towards an extraction well Accounts for depletion of NAPL residuals, lenses or pools. Allows for equilibrium and non-equilibrium partitioning. Different types of sorption isotherms are considered.
VENT3D (1994) David Benson	Three-dimensional, finite difference model of vapor transport and phase distribution of multiple compounds.	Flow and transport of multicomponent mixtures in the vapor phase are simulated. Equilibrium partitioning between phases is assumed.
3DFEMFAT (1998) Scientific Software Group, Washington, D. C.	Three-dimensional, finite element model for flow and transport through saturated/unsaturated, heterogeneous, anisotropic media.	Can simulate infiltration, wellhead protection, agricultural pesticides, sanitary landfills, radionuclide and hazardous waste disposal sites, density induced flow and transport
BIOF&T 3-D (1998) Scientific Software Group, Washington, D. C.	Models flow and transport and biodegradation in the saturated/unsaturated zone in 2-D or 3-D, in heterogeneous, anisotropic media.	Models convection, dispersion, diffusion, desorption, and microbial processes based on oxygen-limited, anaerobic, first-order, or Monod biodegradation kinetics as well as anaerobic or first order sequential degradation involving multiple daughter species.
SESOIL (1998) M. Bonazountas Scientific Software Group, Washington, D. C.	Seasonal compartment model which simulates long-term pollutant fate and migration in the unsaturated soil zone.	Computes pollutant masses in water, soil and air phases. Pollutant migration to ground water, and volatilization to ground surface. Pollutant migration due to surface runoff and erosion.

performance. They can also predict post remedial soil concentrations to determine if cleanup goals were met. Some of the compositional models simulate multicomponent mixtures (such as gasoline), which is useful in predicting which components remain in the system after SVE has been applied to the site. Some models assume equilibrium partitioning between the different phases, while others accommodate mass transfer limitations that can hinder SVE performance.

Vapor migration can also be characterized by multiphase flow and transport models such as T2VOC (Falta et al., 1995; McRay and Falta, 1997), which describe the simultaneous flow and transport of contaminants in the different phases (vapor, water, NAPL, and sorbed phases)). These models demand a high degree of computing power and data input. Gathering the data required by these models is usually difficult, but, these models can be useful in describing the migration of different chemical species in complex settings.

Model selection is usually influenced by site data availability. For small leaking underground storage tanks where little data is available, a screening or an air flow model may prove useful. For a larger site with extensive data available from site characterization, a more complex, compositional or multiphase model may be used. Table 9.3 provides a listing of some of the available flow and transport models for the unsaturated/saturated zones.

9.9.2 Description of a Screening Model: Hypervent

Johnson et al. (1988, 1990) have exploited the analogy to ground water flow in developing simple screening models to describe the distribution in pressure around venting wells. Based on the assumption that vapor behaves as an ideal gas, the governing equation for vapor flow for conditions of radial flow, the governing equation can be written as follows:

$$\frac{1}{r}\frac{\partial}{\partial r}\left(r\frac{\partial P'}{\partial r}\right)=\left(\frac{\theta_a \mu}{kP_{\text{atm}}}\right)\frac{\partial P'}{\partial t} \tag{9.31}$$

where P' is the deviation of pressure from the reference pressure P_{atm}, k is soil permeability, μ is the vapor viscosity, θ_a is vapor filled porosity, and t is time. When Eq. (9.31) is solved with appropriate boundary conditions, with b as the thickness of the unconfined zone and r as the radial distance from the well to the point of interest,

$$P' = \frac{Q}{4\pi b(k/\mu)}\text{W}(u) \text{ where } u = r^2\theta_a\mu/4kP_{\text{atm}}t \tag{9.32}$$

and W(u) is the well function of u, which is a commonly tabulated function.

Calculations with Eq. (9.32) show that for sandy soils (10<k<100 darcys), the pressure distribution approximates a steady state in one to seven days. Thus, it is appropriate to model pressure distributions using a steady state solution to the governing flow equation. For the following set of boundary conditions: $P = P_w$ at $r = R_w$ and $P = P_{\text{atm}}$ at $r = R_l$, where

P_w is the pressure at the well with radius R_w and P_{atm} is the ambient pressure at the radius of influence R_l.

Johnson et al. (1988) provide the following solution to the steady-state equation for radial flow

$$P^2(r) - P_w^2 = \left(P_{\text{atm}}^2 - P_w^2\right)\frac{\ln(r/R_w)}{\ln(R_l/R_w)} \tag{9.33}$$

As Johnson et al. (1988) point out, while not explicitly represented in Eq. (9.33), the properties of the soil do influence the steady-state pressure distribution because the radius of influence (R_l) does vary as a function of permeability and layering. Johnson et al. (1988) develop corresponding solutions for radial darcy velocity and volumetric flow rate for this steady-state case. The latter of these solutions provides a useful way to determine what the theoretical maximum air flow is to a vapor extraction well and is written

$$Q = H\pi\frac{k}{\mu}P_w\frac{[1-(P_{\text{atm}}/P_w)^2]}{\ln(R_w/R_l)} \tag{9.34}$$

where H is the total length of the screen. Just as is the case with well hydraulics, these kinds of analytical equations form the basis not only for predictive analysis, but also for well testing methods for permeability estimations.

Analytical solutions are most useful for screening purposes and for exploring the relationships among variables; however, their practical applicability is limited to simple problems. An alternative way of solving differential equations like Eq. (9.31) is with powerful numerical models. Numerical models are effective in modeling complicated problems of the type commonly encountered in practice.

By analogy with problems involving ground water flow to wells, the general pattern of air circulation will be influenced by features of the fluid being circulated, the geologic system and the well system used to withdraw and inject air. The permeability is the most important of all the parameters that influence flow. Ultimately, it is the permeability that determines the efficacy of vapor extraction because flow rates at steady state for a well under a specified vacuum are a direct function of permeability. Vapor extraction, to be practically useful, requires some minimal rate of air circulation, which may not be feasible in some low permeability units.

From an analytical model, Johnson et al. (1990) developed a series of relationships between permeability and flow rate (Figure 9.11). For a given vacuum in the extraction well, the steady-state rate of air flow is a linear function of permeability (log scales). An increase in the vacuum (smaller P_w) at a given permeability will increase the air flow. However, the maximum change that might be expected is about an order of magnitude in flow rate. It is well known from ground water flow theory that variability in permeability plays an important role in controlling the pattern of flow. This is also the case for patterns of air circula-

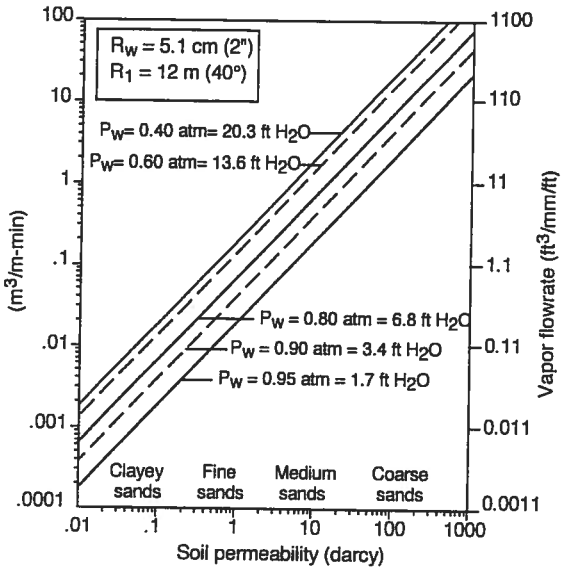

(ft H_2O) denote vacuums expressed as equivalent water column heights

Figure 9.11 Predicted steady-state rates of air flow per unit length of well screen from a vapor extraction well for a range of permeabilities and applied vacuums (Pw). Source: Johnson et al., 1990.

tion. Most circulation will occur through the most permeable zones for a layered system, and this can have a profound effect on the rate and efficiency of cleanup schemes.

Features of the design of the system as a whole also control air circulation. The most important factors in this respect include: (1) the flow rates in the injection/extraction wells,(2) the types and locations of wells in a multiwell system, and (3) the presence of a surface seal. For a single vacuum well, Figure 9.11 illustrates how reducing P_w increases the air withdrawal rate. Similarly, adding more wells to the system will also do the same. Furthermore, the pattern of air circulation can be controlled by the types and locations of the wells. Hypervent (Johnson, 1991) is a screening tool used to determine the potential feasibility of SVE as a remedial option at contaminated sites. It is available free of charge from USEPA and can run on PCs and Apple Macintosh. The model runs in hypertext framework, which consists of several screens that are linked to other screens that provide information, text, files, pictures or calculation sheets. Some of the screens contain tips and diagrams on SVE operation and design, while others prompt the user for input and analytical calculations. The model is based on the Johnson et al. (1990), article.

Vapor Concentrations and Removal Rates. A simplistic equilibrium-based model is used to assess how effective soil venting may be used for remediating a site with a spill of given composition. The total mole balance on each component i is given by:

$$M_i = \frac{z_i P \theta_a V}{RT} + x_i M_{HC} + y_i M_{H_2O} + k_i y_i \frac{M_{soil}}{M_{w,H_2O}} \tag{9.35}$$

where x_i is the mole fraction of component i in free liquid phase, z_i is the mole fraction of component i, in the vapor phase, P is the total vapor pressure [atm], V is the volume of contaminated soil (cm^3), R is the universal gas constant [82.1 cm^3/mole-K], T is the absolute temperature in soil [K], $M_{HC}$is the total moles in free liquid phase, M_{H_2O} is the total moles in soil moisture phase, y_i is the mole fraction of i dissolved in soil moisture, k_i is the sorption coefficient for i, M_{soil} is the total mass of contaminated soil [g], and M_{w,H_2O} is the molecular weight of H_2O.

The vapor concentrations are calculated using Raoult's Law, or linear partitioning depending on the phases present:

$$\text{Raoult's Law: } C_i^a = \frac{x_i P_i^v MW_i}{RT} \tag{9.36}$$

$$\text{Linear Partitioning: } C_i^a = \frac{HC_{i,soil}}{\left[\left(\frac{H\theta_a}{\rho_{soil}} + \theta + k_i\right)\right]} \tag{9.37}$$

where C_i^a is the concentration in the vapor phase [g/cm^3], P_i^v is the component vapor pressure [$g/cm\text{-}s^2$], MW_i is the component molecular weight [g/mole], H is Henry's Law constant (dimensionless), $C_{i,soil}$ is the component concentration in soil [g/g], θ is the moisture content [cm^3/g], and ρ_{soil} is the soil density [cm^3/g].

Removal rates are calculated by QC_i^a, and the volume of vapor required to achieve desired cleanup is calculated by QT/(Spill mass). The minimum number of extraction wells required is calculated by:

$$\frac{\{\text{Volume of required vapor}\} \bullet \{\text{Spill mass}\}}{\{\text{Desired cleanup time}\} \bullet Q}$$

Hypervent will not completely design an SVE system, give the length of required operation, or predict the behavior of the system. Hypervent data requirements include soil permeability, extraction well radius, screened interval, well radius, radius of influence, contaminant composition other than gasoline, contaminant mass, contaminant concentration, com-

ponents' vapor pressure, components' molecular weights, desired cleanup time, air pumping test data, and radius of contaminated zone. Hypervent output provides extraction well flowrates, contaminant removal rates, soil permeability from pumping tests, if desired, and an optimum number of extraction wells.

Example 9.3 VAPOR EXTRACTION COMPUTATIONS

Johnson et al. (1988) examined mass removals (Figure 9.12) for a hypothetical case in which 400 gal (approximately 1500 L) of gasoline were spilled into 1412 ft^3 of soil at a 10% moisture content. This spill provides a residual saturation of 2% gasoline by dry weight or 20,000 ppm total petroleum content. Other conditions specified include: a soil bulk density of 1.5 gm/cm^3, a porosity of 0.40, an organic carbon fraction (f_{oc}) of 0.01, an air flow rate of 20 ft^3/min, a soil temperature of 60 °F, and a relative humidity for the incoming air of 100%. The problem assumes that 25% of the circulating air passes through the spill. Thus, component concentrations in the vapor extraction well will be at equilibrium for an air flow of 5 ft^3/m, which is the value used in subsequent calculations. Also required for the calculation is information about the compounds found in gasoline, their molecular weights and mass fractions, and their physical properties (see Johnson et al., 1988).

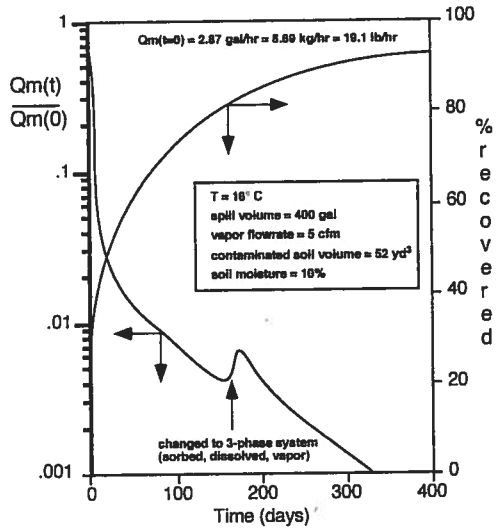

Figure 9.12 Predicted mass loss rates for a hypothetical venting operation. Source: Johnson et al., 1990.

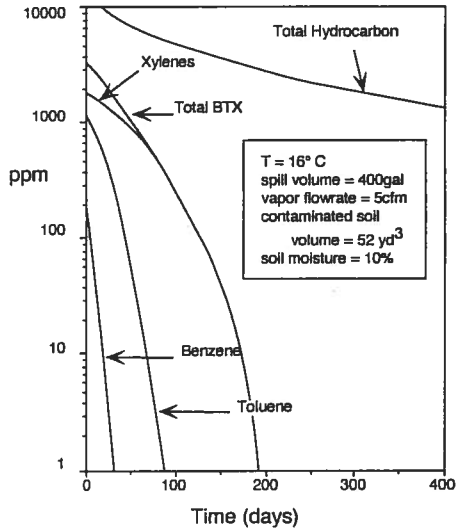

Figure 9.13 Predicted soil concentrations of hydrocarbons for a hypothetical venting operation. Source: Johnson et al., 1990.

The total rate of mass loss from vapor extraction for the entire gasoline mixtures is the sum of the mass loss rates C_iQ for the compounds. The total mass loss rate as a ratio of the initial mass loss rate is plotted versus time in Figure 9.12. Also depicted in the figure is the cumulative percentage of the initial spill recovered as a function of time. The example clearly shows how the rate of mass loss decreases with time as the most volatile components are removed from the mixture. Figure 9.13 displays the time variation in the soil concentrations of a number of the most volatile compounds in gasoline. The pattern of removal rates (i.e., benzene > toluene > xylenes) is explained by the respective vapor pressures (i.e., 0.10 > 0.029 > 0.0066 to 0.0088 atm). At the end of 400 days, the residual product consists mainly of the larger molecular weight compounds in gasoline having vapor pressures in general less than 0.005 atm. Thus, about 25 days are required to recover half of the original spill mass, but about 400 days are required to collect 90%.

9.9.3 Description of a Flow and Transport Model: VENT3D

VENT3D, is a 3-D, finite-difference code for vapor flow and transport (Benson, 1994; Benson et al., 1993). VENT3D solves the 3-D vapor flow and transport equation for a multicomponent mixture, and describes the movement of compounds in the vapor phase and the

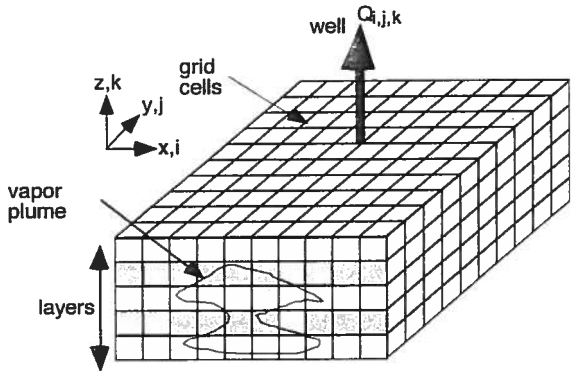

Figure 9.14 Schematic of VENT3D structure.

phase distribution of each compound in the other three phases (NAPL phase, dissolved phase, and sorbed phase). The equilibrium four-phase distribution of each compound in the mixture is solved between vapor phase moving periods. The model domain is divided into an orthogonal grid in the x and y plane, and into several layers in the z direction. Thus, the domain is divided into blocks, each block may be given unique properties such as permeability or contaminant concentrations. Extraction and injection wells can be simulated. Figure 9.14 shows a schematic diagram of the code structure. The code was compiled for a Sun Sparc Workstation.

The gas phase is the only moving phase, and gas transport occurs due to diffusion in the gas phase and advection in case of forced venting, where molecular diffusion is calculated as a function of the air diffusion coefficient and air saturation. The model does not account for interphase mass transfer. Vapor pressure is entered at 20 °C and is calculated by the model at higher and lower temperature. The model assumptions are as follows:

- equilibrium partitioning between the gas phase and all other phases (dissolved, sorbed, and NAPL)
- the system is isothermal
- constant gas viscosity
- linear sorption
- air is incompressible
- elevation head is ignored compared to pressure head

A detailed example of vapor extraction modeling using VENT 3D is presented in Chapter 13.

Flow Algorithm. Elevation head is ignored compared to pressure head in the formulation of soil gas head. Hence, the 3-D steady-state gas flow equation based on the principle of mass conservation is as follows:

$$\frac{\partial}{\partial x}\left(k_x \frac{\partial P^2}{\partial x}\right)+\frac{\partial}{\partial y}\left(k_y \frac{\partial P^2}{\partial y}\right)+\frac{\partial}{\partial z}\left(k_z \frac{\partial P^2}{\partial z}\right)=\frac{2\mu WRT}{dx \cdot dy \cdot dz \cdot MW} \tag{9.38}$$

where k is the soil vapor permeability tensor [L^2], P is the soil-gas pressure [$ML^{-1}T^{-2}$], μ is the soil-gas viscosity [$ML^{-1}T^{-1}$], W is the vapor mass flux source/sink [MT^{-1}], R is the universal gas constant [$ML^2T^{-2}mole^{-1}K^{-1}$], T is the temperature [K], and MW is the molecular weight of soil-gas [$M \cdot mole^{-1}$].

To solve the flow equation, an orthogonal grid is used to discretize the model domain and boundary conditions should be specified. The bottom layer is always assumed as a no-flow boundary, the top layer is specified by the user as a no-flow boundary (sealed surface) or an open to the atmosphere boundary. The lateral boundary can also be open or closed to the surrounding.

The flow equation is solved by finite differences for pressures in between gridlines. The effective permeability, which is the permeability of the porous medium to each fluid, is calculated as a function of the relative saturation of this fluid using the Brooks and Corey (1964) relationship. Because the volumes of liquid contaminant and soil moisture in the pores are changing all the time during a simulation, the effective permeability should be recalculated.

$$k = k^*\left(\frac{\theta_a}{n}\right)^3 \tag{9.39}$$

where k^* is the intrinsic permeability of the porous media [L^2], θ_a is the air filled porosity [dimensionless], and n is the porosity [dimensionless]. With the Brooks and Corey expression the permeability field can be re-calculated at each time step to reflect the ongoing depletion of pore fluids. The time step is computed internally by the model. Hence, the gas pressure is calculated in between blocks, and the interblock gas flow v is also determined by Darcy's law in the x,y,z directions as follows:

$$v_x = \frac{k_x}{\mu\theta_a}\frac{\partial P_x}{\partial x}, v_y = \frac{k_y}{\mu\theta_a}\frac{\partial P_y}{\partial y}, v_z = \frac{k_z}{\mu\theta_a}\frac{\partial P_z}{\partial z} \tag{9.40}$$

Transport Algorithm. The model describes the movement of compounds in the vapor phase and their phase distribution. The flux of each chemical compound in the vapor phase is composed of the advective motion of soil gas and the dispersive flux of that compound. The change in molar concentration within the differential element with respect to

time is the difference between the sum of directional fluxes and a chemical source/sink as represented by Eq. (9.41) (Benson, 1994). The dispersive flux consists of the diffusive flux due to molecular diffusion and the velocity dependent hydrodynamic dispersion as shown in Eq. (9.42).

$$\frac{\partial M_i}{\partial t} + F_i = \nabla \cdot \left[D_i \nabla (C_i) - \nabla (q C_i) \right] \tag{9.41}$$

where M_i is the total molar concentration of each compound in mixture [mole/L^3], C_i is the molar concentration of each compound [mole/L^3], q is the vapor discharge vector [L/T], F_i is the volumetric molar loss/addition rate of compound [mole·L^{-3}T^{-1}], and D_i is the dispersion tensor [L^2/T], as follows:

$$D_i = D_m I + \alpha_{xyz} \frac{q_x q_y}{\theta_a \bar{q}} \tag{9.42}$$

where D_m is the molecular diffusion coefficient [L^2/T], I is the identity vector, α_{xyz} is the vapor dispersivity [L], q_x, q_y are the vapor flows in x and y directions [L/T], and $\bar{q}$ is the magnitude of the discharge vector [L/T]. The molecular diffusion is a function of air diffusion coefficients and is determined by the Millington and Quirk expression represented by Eq. (9.43). The molecular diffusion is a function of air filled porosity, which changes with movement of compounds and fluid saturation, as follows:

$$D_m = D_0 \frac{\theta_a^{10/3}}{n^2} \tag{9.43}$$

where D_0 is the free air diffusion coefficient [L^2/T], θ_a is the air-filled porosity, and n is the total porosity.

Knowing the flows between the blocks, the 3-D advection-dispersion equation is solved by finite-difference for each chemical compound. The advective transport term is solved by three different algorithms: central weighted scheme if diffusive flux is larger than advective flux; single-point upwind if advective flux is larger than diffusive flux; third order, with variable weighting of gradients, if dispersive flux is high. The last algorithm alleviates oscillation and numerical dispersion with sharp fronts. After the chemical compounds have been moved by the appropriate advective algorithm, each node carries a new concentration of each compound. The dispersive term in Eq. (9.42) is evaluated using standard explicit finite-differences.

In case of a soil contaminated with a number of chemical compounds, the contaminants are present in the gas phase, dissolved in the soil moisture, sorbed to the soil, and forming a separate nonaqueous phase. Equilibrium partitioning is assumed between the different phases for each compound. As vapors migrate between time steps, the vapor composition and concentrations will change and nonequilibrium conditions will occur between the

existing phases. The total molar concentration of each compound is expressed as a function of the vapor concentration and the sum of the molar concentrations in the four phases as shown in Eq. (9.44). The four terms on the right-hand side of Eq. (9.44) represent the contribution to the total soil contamination of the vapor phase, the NAPL phase, the dissolved phase and the sorbed phase respectively. When a separate phase is present, the sum of the mole fractions of the non-aqueous phase liquid has to be equal to 1.0 as represented by Eq. (9.45). Between time steps, moles of each compound are moved into and out of each finite-difference cell. By solving Eq. (9.44) and Eq. (9.45) iteratively, equilibrium is re-calculated at the end of each time step.

$$M_i = C_i \left[\theta_a + \frac{M_{HC} RT}{P_i^v} + \frac{M_{H_2O} RT}{\alpha_i P_i^v} + \frac{K_d^i \rho RT \delta_{H_2O}}{\alpha_i P_i^v MW_{H_2O}} \right] \tag{9.44}$$

subject to

$$\sum_{i=1}^{\#\text{compounds}} \frac{C_i RT}{P_i^v} = 1 \tag{9.45}$$

where M_{HC} is the molar concentration of NAPL phase in soil [mole/L^3], P_i^v is the compound vapor pressure [atm], M_{H_2O} is the molar concentration of dissolved phase [mole/L^3], γ_i is the activity coefficient of compound in water [dimensionless], K_d^i is the distribution coefficient of compound [dimensionless], ρ is the soil density [M/L^3], MW_{H_2O} is the molecular weight of water [18 gm/mole], and δ_{H_2O} is the soil moisture flag = 1 if present, 0 if not present.

To solve the equilibrium Eq. (9.44), it is necessary to estimate activity coefficients and component vapor pressures at the temperature of interest. Activity coefficients are obtained using Eq. (9.46):

$$\gamma_i = \frac{MC_{H_2O} \times MW_i}{S_i} \tag{9.46}$$

where MC_{H_2O} is the molar concentration of water (55.5 mole/L^3), MW_i is the molecular weight of compound i (M/mole), and S_i is the pure component solubility of compound i (M/L^3). For gases the activity is calculated by multiplying Eq. (9.46) by [1 atm / P^v].

Vapor pressures at temperatures of interest are calculated using the Claussius-Clapyron equation.

$$P^v = P^v_{20°C} \exp\left[\frac{T_b \cdot 20°\text{C}}{(T_b - 20°\text{C})}\left(\frac{1}{T} - \frac{1}{20°\text{C}}\right)\ln\left(\frac{P^v_{20°\text{C}}}{1\text{ atm}}\right)\right] \quad (9.47)$$

where $P^v_{20°C}$ is the vapor pressure of compound at 20 °C [atm], T_b is the boiling point of compound [°C], and T is the temperature of interest [°C].

VENT3D assumes a linear sorption isotherm between the dissolved and sorbed phases.

$$K^i_d = 0.63 K^i_{ow} f_{oc} \quad (9.48)$$

where K^i_{ow} is the octanol/water partition coefficient of compound [M/M], and f_{oc} is the fraction of organic carbon [M/M].

Mass Balance Calculations. The mass of each contaminant compound remaining within the model has the potential of changing with every time step. The mass balance within the program is a measure of the accuracy of the simulation. The model computes an internal time step size to ensure stability and low mass balance errors. Three different methods are used to calculate the time step size: the dispersion rate, the pumping rates, and the soil gas velocity. The model selects the smallest time step size of the three at each time step. Mass balance errors are computed at the end of each time step by comparing the mass removed, the mass remaining, and the initial mass. The mass balance equations are taken from Konikow and Bredehoeft (1978). A detailed application of VENT3D to a field site at Hill AFB in Utah is shown in Section 13.9.3.

Data Requirement. *Parameters common to domain*: contaminant composition, fraction of organic carbon, bulk density, and grid dimensions. *Parameters common to each grid block*: permeability, contaminant concentration, extraction/injection rate, and injected air humidity. *Parameters common to each layer*: permeability anisotropy, layer depth, porosity, and moisture content. *Boundary conditions*: ground surface open or closed to atmosphere; lateral boundaries at atmospheric pressure, no flux or known flux; bottom surface represents water table, i.e., no flux.

Model Output. *Parameters common to domain*: initial moles, pumped moles, domain loss moles, remaining moles for each compound, initial total mass, total pumped mass, mass lost from domain, remaining mass, and mass balance errors. *Parameters common to each grid block*: pressure, vacuum, horizontal and vertical air permeability, discharge, remaining total contaminant mass in soil, remaining mass for each compound in soil, remaining soil gas concentrations, and off-gas concentrations for each compound at extraction wells.

Example 9.4. VAPOR EXTRACTION APPLICATION

An example of a VENT3D application to a contaminated site in California is presented by Jordan et al. (1995). The site is formed of different layers, a coarse sand layer at 10 to 30 ft below ground surface (BGS), a silt and clay rich layer at 30 to 40 ft BGS and a well sorted sand below the silty/clayey layer where a water table exists. The highest contamination was found just above the water table. During the field study, vapor was withdrawn from one well for 275 days, followed by withdrawal from other wells at different locations for 950 days. The site was modeled in two dimensions using VENT 3D. A plot of the measured soil vapor total petroleum hydrocarbon (TPH) concentrations and simulated concentrations are shown in Figure 9.15, and demonstrate the usefulness of the model.

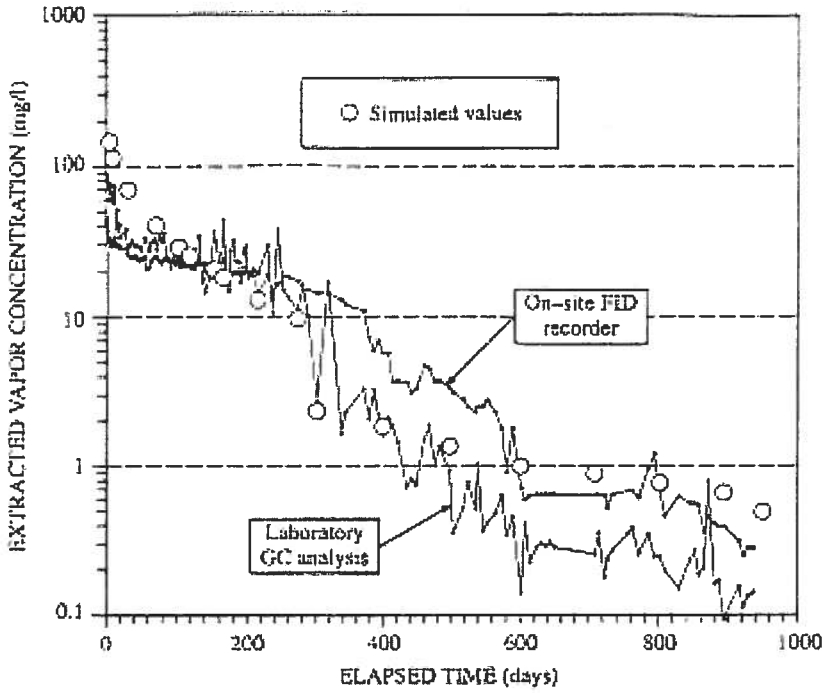

Figure 9.15 Simulated and measured decline of TPH concentrations in vapor extracted from the Costa Mesa sites. Measured values are represented by connected points. Simulated values are represented by large open circles.

SUMMARY

Flow and transport processes in the unsaturated zone are much more complex than in the saturated zone due to the effect of capillary forces, nonlinear soil characteristics, and the presence of four phases of interest: soil, water, air, and NAPL. Being bound at its top by the ground surface and below by ground water, the unsaturated zone serves as a conduit through which liquid and gaseous contaminants can reach the underlying aquifers and overlying ground surface. Contaminants in the residual phase can reach the water table by dissolution, infiltration, vapor migration, or water table fluctuation. Vapor flow to ground surface or basements of structures may occur by pressure and concentration gradients. Vapor transport is governed by diffusion, advection, dispersion, and reactions. A number of screening, compositional, and multiphase transport models have been developed to simulate processes in the unsaturated zone. Hypervent is an example of a screening model, and VENT3D is an example of a compositional model.

REFERENCES

Anderson, M. P., and W. W. Woessner, "Applied Ground Water Modeling: Simulation of Flow and Advective Transport." New York, Academic Press, 1992.

Armstrong, J. E., Frind, E. O., and R. D. McClellan, "Nonequilibrium Mass Transfer between the Vapor, Aqueous, and Solid Phases in the Unsaturated Soils during Vapor Extraction." *Water Resources Res.*, 30(2), 355-368, 1994.

Baehr, A. L., and C. J. Bruell, "Application of the Stefan-Maxwell Equations to Determine Limitations of Fick's Law when Modeling Organic Vapor Transport in Sand Columns" *Water Resources Res.*, 26(6), 1155-1163, 1990.

Bear, J., *Hydraulics of Ground water*, New York, McGraw Hill, 1979.

Bedient, P. B., and W. C. Huber, *Hydrology and Floodplain Analysis*, Reading, MA, Addison-Wesley, 1992.

Benson, D. A., Huntley, D., and P. C. Johnson, "Modeling Vapor Extraction and General Transport in the Presence of NAPL Mixtures and Nonideal Conditions" *Ground Water*, 31(3), 437-445, 1993.

Benson, D., "User's Manual to VENT3D: A Three-Dimensional Multi-Compound, Multi-Phase Partitioning Vapor Transport Model," 1994.

Brooks, R. H. and A. T. Corey, "Hydraulic Properties of Porous Media," *Hydrol. Pap. 3*, Colo. State Univ., Fort Collins, pp. 27, 1964.

Brusseau, M. L., "Transport of Organic Chemicals by Gas Advection in Structured or Heterogeneous Porous Media: Development of a Model and Application to Column Experiments," *Water Resources Res.*, 27(12), 3189-3199, 1991.

Brusseau, M. L., "Transport of Reactive Contaminants in Heterogeneous Porous Media," *Reviews of Geophysics*, 32(3), 285-313, 1994.

Carlisle, V. W., C. T. Hallmark, F. Sodek III, R. E. Caldwell, L. C. Hammond and V. E. Berkheiser, "Characterization Data For Selected Florida Soils," Soil Characterization Laboratory, Soil Science Department, Gainesville, University of Florida, 1981.

Clapp, R. B. and G. M. Hornberger, "Empirical Equations For Some Soil Hydraulic Properties," *Water Resources Res.*, Vol. 14, pp. 601-604, 1978.

Charbeneau, R. J., "Kinematic Models for Moisture and Solute Transport," *Water Resources Res.*, Vol. 20(6), pp. 699, 706, 1984.

Charbeneau, R. J., "Groundwater Hydraulics and Pollutant Transport," Course Notes, University of Texas, Austin, Texas, 1990.

Charbeneau, R. J., and D. E. Daniel, "Contaminant Transport in Unsaturated Flow," *Hand Book of Hydrology*, Chapter 15, D. R. Maidment, ed., New York, McGraw-Hill, 1993.

Chow, V. T., D. R. Maidment and L. W. Mays, *Applied Hydrology*, New York, McGraw-Hill, 1988.

Conant, B. H., Gillham, R. W., and C. A. Mendoza, "Vapor Transport of TCE in the Unsaturated Zone: Field and Numerical Modeling Investigations." *Water Resources Res.*, 32(1), 9-22, 1996.

Davidson, J. M., D. R. Nielsen and J. Biggar, "The Dependency of Soil Water Uptake and Release Upon the Applied Press Increment," *Soil Sci. Soc. Am. Proc.*, Vol. 30(3), pp. 298-304, 1966.

Enfield, C. G., D. M. Walters, J. T. Wilson and M. Piwoni, "Behavior of Organic Pollutants During Rapid Infiltration of Wastewater Into Soil: II. Mathematical Description of Transport and Transformation," submitted for publication, *Journal of Environmental Quality*, 1985.

Falta, R. W., K. Pruess, S. Finsterle, and A. Battistelli, "T2VOC User's Guide," Earth Sciences Dept., Clemson University; Earth Sciences Dept., University of California, Berkeley, 1995.

Falta, R. W., Javandel, I., Pruess, K., and P. A. Witherspoon, "Density-Driven Flow of Gas in the Unsaturated Zone due to the Evaporation of Volatile Organic Compounds." *Water Resources Res.*, 25(10), 2159-2169, 1989.

Fetter, C. W., *Contaminant Hydrogeology*, Upper Saddle River, NJ, Prentice Hall, 1999.

Freeze, R. A., "The Mechanism of Natural Groundwater recharge and Discharge: 1. One-dimensional, Vertical, Unsteady, Unsaturated Flow above a Recharging or Discharging Groundwater Flow System," *Water Resources Res.* 5:153-171, 1969.

Freeze, R. A., " Three-dimensional, Transient, Saturated-Unsaturated Flow in a Groundwater Basin," *Water Resources Res.* 7:347-366, 1971.

Freeze, R. A., and J. A. Cherry, *Groundwater*, Prentice Hall, Englewood Cliffs, NJ, 1979.

Gierke, J. S., Hutzler, N. J., and J. C. Crittenden, "Modeling the Movement of Volatile Organic Chemicals in Columns of Unsaturated Soil." *Water Resources Res.*, 26(7), 1529-1547.

Green, W. H. and G. A. Ampt, 1911, "Studies of Soil Physics, 1: The Flow of Air and Water Through Soils," *J. of Agriculture Science*, Vol. 4, No. 1, pp. 1-24.

Gupta, S. C. and W. E. Larson, 1979, "Estimating Soil Water Retention Characteristics from Particle Size Distribution, Organic Matter Percent, and Bulk Density," *Water Resources Res.*, vol. 15, pp. 1633-1635.

Guymon, Gary L., *Unsaturated Zone Hydrology*, Englewood Cliffs, NJ, Prentice Hall, 1994.

Hinchee, R. E., et al., "Underground Fuel Contamination, Investigation, and Remediation a Risk Assessment Approach to How Clean Is Clean," *Proceedings* Petroleum Hydrocarbons and Organic Chemicals in Ground Water, Dublin, OH, NWWA, pp. 539-563, 1986.

Ho, C. K., and K. S. Udell, "An Experimental Investigation of Air Venting of Volatile Liquid Hydrocarbon Mixtures from Homogeneous Porous Media." *Journal of Contaminant Hydrology*, 11, 291-316, 1992.

Hoag, G. H., and M. C. Marley, "Gasoline Residual Saturation in Unsaturated Uniform Aquifer Materials." *Environmental Engineering*, 112(3), 586-604, 1986.

Holtan, H. N., "A Concept for Infiltration Estimates in Watershed Engineering," *USDA Bull.*, 41-51, 1961.

Horton, R. E., "An Approach toward a Physical Interpretation of Infiltration Capacity," *Soil Science Society Amer. J.* 5:399-417, 1940.

"Approach toward a Physical Interpretation of Infiltration-Capacity," *Soil Sci, Soc. Am. J.*, vol. 5, pp. 399-417.

Johnson, P. C., Kemblowski, J. D., and J. D. Colthart, "Practical Screening Models for Soil Venting Applications." *Petroleum Hydrocarbons and Organic Chemicals in Ground Water*, Houston, Texas, 521-546, 1988.

Johnson, P. C., C. C. Stanley, M. W. Kemblowski, D. L. Byers, and J. D. Colthart, "A practical approach to the design, operation, and monitoring of in-situ soil-venting systems," *Ground Water Monitoring Review*, 10:2:159-178, 1990a.

Johnson, P. C., Hyper Ventilate User's Manual, Shell Oil Company, 1991.

Jordan, D. L., Mercer, J. W., and R. M. Cohen, "Review of Mathematical Modeling for Evaluating Soil Vapor Extraction Systems." *540/R-95/513*, National Risk Management Research Laboratory, Office of Research and Development, USEPA, 1995.

Jury, W. A., W. F. Spencer and W. J. Farmer, "Chapter 4: Chemical Transport Modeling: Current Approaches and Unresolved Problems," *Chemical Mobility and Reactivity in Soil Systems*, ASA, Madison, WI, pp. 49-64, 1983.

Klute, A., and C. Dirksen, "Hydraulic Conductivity and Diffusivity--Laboratory Methods," in A. Klute, ed., *Methods of Soil Analysis, Part I – Physical and Mineralogical Methods*, American Society of Agronomy Monograph 9, 2d ed., pp. 687-734, 1986.

Konikow, L. F., and T. D. Bredehoeft, "Computer Model of Two-Dimensional Solute Transport and Dispersion in Ground Water," Techniques of Water Resources Investigations of the United States Geological Survey, 90, 1978.

Marley, M. C. and G. E. Hoag, Induced soil venting for the recovery/restoration of gasoline hydrocarbons in the vadose zone. Petroleum Hydrocarbons and Organic Chemicals in Ground Water--Prevention, Detection and Restoration, NWWA, Dublin, OH, pp. 473-503, 1984.

Massmann, J. W., "Applying Ground Water Flow Models in Vapor Extraction System Design," *Journal of Environmental Engineering*, 115(1), 129-149, 1989.

Massmann, J., and D. F. Farrier, "Effects of Atmospheric Pressures on Gas Transport in the Vadose Zone." *Water Resources Res.*, 28(3), 777-791, 1992.

McCray, J. E., and R. W. Falta, "Numerical Simulation of Air Sparging for Remediation of NAPL Contamination," *Ground Water*, 35(1), 99-110, 1997.

McCarthy, K. A., and R. L. Johnson, "Transport of Volatile Organic Compounds Across the Capillary Fringe." *Water Resources Res.*, 29(6), 1675-1683, 1993.

Mein, R. G. and C. L. Larson, "Modeling Infiltration During a Steady Rain," *Water Resources Res.*, Vol. 9, No. 2, pp. 384-394, 1973.

Mendoza, C., A., and E. O. Frind, "Advective-Dispersive Transport of Dense Organic Vapors in the Unsaturated Zone: 1. Model Development." *Water Resources Res.*, 26(3), 379-387, 1990a.

Mendoza, C. A., and E. O. Frind, "Advective-Dispersive Transport of Dense Organic Vapors in the Unsaturated Zone: 2. Sensitivity Analysis." *Water Resources Res.*, 26(3), 388-398, 1990b.

Metcalfe, D. E., and G. J. Farquhar, "Modeling Gas Migration through Unsaturated Soils from Waste Disposal Sites," *Water Air and Soil Pollution*, 32, 247-259, 1987.

Millington R. J., and J. M. Quirk, "Permeability of Porous Media," *Trans Faraday Soc.* 57:1200-1207, 1961.

Neuman, S. P., "Saturated-Unsaturated Seepage by Finite Elements," *J. Hydraul. Eng.*, Vol. 99 (HY12), pp. 2233-2251, 1986.

Nielsen, D. R., M. Th. van Genuchten, and J. W. Biggar, "Water Flow and Solute Transport Processes in the Unsaturated Zone," *Water Resour. Res.*, vol. 22, no. 9, pp. 89S-108S, 1986.

Nofziger, D. L., J. R. Williams and T. E. Short, "Interactive Simulation of the Fate of Hazardous Chemicals During Land Treatment of Oily Wastes," EPA/600/8-88/001, 1988.

Nofziger D. L., K. Rajender, S. K. Nayudu and P. Su, "Chemflo: One-Dimensional Water and Chemical Movement in Unsaturated Soils," EPA/600/8-89/076, 1989.

Olson, R. S., and D. E. Daniel, "Measurement of Hydraulic Conductivity of Fine-grained Soils," in T. F. Zimmie and C. O. Riggs, eds., *Permeability and Groundwater Contaminant Transport*, STP 746, Philadelphia, American Society of Testing and Materials, pp. 18-64, 1981.

Panday, S. and M. T. Corapcioglu, "Reservoir Transport Equations by Compositional Approach," *Trans. Porous Media*, Vol. 4, pp. 369-393, 1989.

Pankow, J. F. and J. A. Cherry, Dense Chlorinated Solvents and Other DNAPLS in Ground Water: History, Behavior, and Remediation, Portland, Oregon, Waterloo Press, 1996.

Philip, J. R. and D. A. de Vries, "Moisture Movement in Porous Media Under Temperature Gradients," *Eos Trans*, AGU, Vol. 38(2), pp. 222-232, 1957.

Powers, S. E., C. O. Loureiro, L. M. Abriola, and W. J. Weber, "Theoretical Study of the Significance of Nonequilibrium Dissolution of Nonaqueous Phase Liquids in Subsurface Systems," *Water Resources Res.*, 27(4), 463-477, 1991.

Richards, L. A., "Capillary Conduction of Liquids in Porous Mediums," *Physics*, Vol. 1, pp. 318-333, 1931.

Rathfelder, K., Yeh, W. W.-G., and D. Mackay, "Mathematical Simulation of Soil Vapor Extraction Systems: Model Development and Numerical Examples." *Contaminant Hydrology*, 8, 263-297, 1991.

Rathfelder, K., Lang, J. R., and L. M. Abriola, "Soil Vapor Extraction and Bioventing: Applications, Limitations and Future Research Directions," *Reviews of Geophysics, Supplement*, 1067-1081, 1995.

Rawls, W. J., D. L. Brakensiek and N. Miller, "Green-Ampt Infiltration Parameters From Soils Data," *J. Hydraulic Engineering*, ASCE, Vol. 109, No. 1, pp. 62-70, 1983.

Rawls, W. J., Ahuja, L. R., Brakensiek, A., and A. Shirmohammadi, "Infiltration Parameters from Soils Data," *J. Hydraulic Engineering*, American Society of Civil Engineers 109(1):62-70, 1993.

Rubin, J. And R. Steinhardt, "Soil Water Relations During Rain Infiltration, I, Theory," *Soil Sci. Soc. Am. Proc.*, Vol 27(3), Pp. 246-251, 1963.

Soil Conservation Service, *Urban Hydrology for Small Watersheds*, Technical Release 55, pp. 2.5-2.8, 1986.

Short, T. E., "Modeling of Processes in the Unsaturated Zone," in R. C. Loehr and J. F. Malina, Jr., eds., *Land Treatment: A Hazardous Waste Management Alternative*, Water Resources Symposium Number Thirteen, U.S. EPA and University of Texas at Austin, pp. 211-240, 1986.

Short, T. E., "Movement of Contaminants from Oily Wastes during Land Treatment," in E. J. Calabrese and P. J. Kostecki, eds., *Soils Contaminated by Petroleum: Environmental and Public Health Effects*, New York, John S. Wiley and Sons, pp. 317-330, 1988.

Skaggs, R. W. and R. Khaleel, "Chapter 4, Infiltration," *Hydrologic Modeling of Small Watersheds*, C. T. Haan, J. P. Johnson and D. L. Brakensiek (eds.), American Society of Agricultural Engineers, St. Joseph Michigan, Monograph No. 5, 1982.

Sleep, B. E., and J. F. Sykes, "Modeling the Transport of Volatile Organics in Variably Saturated Media." *Water Resources Res.*, 25(1), 81-92, 1989.

Smith, R. E., "Approximate Soil Water Movement by Kinetic Characteristics," *Soil Sci. Soc. Am. J.*, Vol. 47 (1), pp. 3-8, 1983.

Swartzendruber, D., "A Quasi Solution of Richards' Equation for Downward Infiltration of Water into Soil," *Water Resources Res.*, vol. 5, pp. 809-817, 1987.

Thibodeaux, L. J. and S. T. Hwang, "Landfarming of Petroleum Wastes - Modeling of the Air Emissions Problem." *Env. Progress*, 1, Vol. 1, pp. 42-46, 1982.

Van Genuchten, M. Th., "A Closed-Form Equation for Predicting the Hydraulic Conductivity of Unsaturated Soils," *Soil Sci. Soc. Am. J.*, vol. 44, pp. 892-898, 1980.

Verschueren, K., *Handbook of Environmental Data on Organic Chemicals*, New York, Van Nostrand Reinhold, 1983.

CHAPTER 10

NUMERICAL MODELING OF CONTAMINANT TRANSPORT

10.1 INTRODUCTION

A ground water model is a tool designed to represent a simplified version of a real field site. It is an attempt to take our understanding of the physical, chemical, and biological processes and translate them into mathematical terms. The resulting model is only as good as the conceptual understanding of the processes. The goal of modeling is to predict the value of an unknown variable such as head in an aquifer system or the concentration distribution of a given chemical in the aquifer in time and space. Models can be used as:

1. Predictive Tools. These are site specific applications of models with the objective of determining future conditions or the impact of a proposed action on existing conditions in the subsurface.